FACULDADE DE ENGENHARIA DA UNIVERSIDADE DO PORTO

Smart Garment with integrated IMU for monitoring physical activity

Luis Eduardo Ruano Argueta



MSc. Biomedical Engineering

Supervisor: Miguel Velhote Correia, PhD

July 19, 2024

© FEUP, 2024

Smart Garment with integrated IMU for monitoring physical activity

Luis Eduardo Ruano Argueta

MSc. Biomedical Engineering

July 19, 2024

Acknowledgments

During the last year, many people and institutions have made the realization of this research a reality. Among these, I could highlight family and friends who help by showing their unconditional support and always motivating me to achieve better results.

Among the people to highlight, I would like to mention my advisor, Professor Miguel Velhote Correia. During the execution of the entire project, he was the closest point of contact to resolve all my doubts and help resolve any inconvenience that arose during this time. I would also like to highlight the support of INESCTEC, which provided the necessary tools for developing the project in conjunction with the additional motivation generated by a research fund working as a research assistant.

A special thank you to all the people and companies that are part of the TexP@ct project since this is the achievement of teamwork. The great work of the CITEVE team in developing the different prototypes and the constant support from the sports faculty were great in resolving doubts about their metrics and objectives. Additional thanks to the Plux team for providing all the technical knowledge and the development of the hardware that allowed the validation of the algorithms in a virtual as well as a physical environment. We hope this work is a starting point or inspiration for new projects.

Sincerely

Luis

"For the past two weeks you have been reading about a bad break. Yet today I consider myself the luckiest man on the face of the earth."

Lou Gehrig

Contents

1 Introduction **1**
- 1.1 Context and Motivation . . . 1
- 1.2 Objectives . . . 1
- 1.3 Document Structure . . . 2

2 Theoretical Concepts **4**
- 2.1 Inertial Measurement Units . . . 4
  - 2.1.1 Accelerometer . . . 4
  - 2.1.2 Gyroscope . . . 5
  - 2.1.3 Magnetometer . . . 6
- 2.2 Movement Representations . . . 6
  - 2.2.1 Euler Angles . . . 7
  - 2.2.2 Quaternion . . . 8
  - 2.2.3 Axis Angle Representation . . . 9
  - 2.2.4 Rotation Matrix . . . 9
- 2.3 Global Position System . . . 10
- 2.4 Electrocardiogram ECG . . . 10
- 2.5 Machine Learning . . . 13

3 State of the Art Review **14**
- 3.1 Wearables . . . 14
- 3.2 Smart Textiles . . . 14
- 3.3 Outdoor and Indoor Tracking Vests . . . 16
- 3.4 Metrics from Sports-Science Perspective . . . 17
- 3.5 Biomechanical Movements . . . 18
- 3.6 Characterization of Movements . . . 21
  - 3.6.1 Describing Walking and Running through Velocity and Distance . . . 21
  - 3.6.2 Describing Jumping through Time, Height, Force and Power . . . 23
- 3.7 External and Internal Workloads . . . 24
  - 3.7.1 External Loads . . . 24
  - 3.7.2 Internal Loads . . . 26

4 Methodology **29**
- 4.1 Jump . . . 29
- 4.2 Running . . . 34

5 Results and Discussion **42**
5.1 Vertical Jump 42
5.2 Walk and Run 48

6 Conclusions and Next Steps **56**

References **59**

A IMU Specifications **73**

List of Figures

2.1 Single Moving Mass Accelerator 5
2.2 Gyroscope Internal Structure 6
2.3 Hall Effect induced with current on Magnetometer 7
2.4 Airplane Orientation using Euler Angles 8
2.5 Axis Angle Representation 9
2.6 ECG signal with (P, Q, R, S, T) points 11
2.7 Workflow for ECG Acquisition Signal 11

3.1 StatSports Apex Athlete Series 17
3.2 Work Flow for Activity Recognition using Traditional Machine Learning Approach 20
3.3 Work Flow for Activity Recognition using Deep Learning Machine Learning Approach 20

4.1 Low Limb representation with IMU sensor location for dataset Maule 30
4.2 Optical markers location for dataset Maule 31
4.3 Worn Vest with the placement of the IMU Sensor on t8 section in calibration position 32
4.4 XSens Front and Back Location of IMU'S 33
4.5 Counter Movement Jump Phases with IMU 34
4.6 Hankyong National University of South Korea Dataset Location for IMU on the subject 36
4.7 Hasso Plattner Institute Dataset Location for IMU on subject 37
4.8 CWT Application on the Vertical Accelerometer Signal Walk 38
4.9 Workflow for Vertical Jump Metrics 40
4.10 Workflow for Walk, Run Metrics 41

5.1 Data Representation for CMJ and Workflow on Maule Dataset 43
5.2 Bland-Altman Charts for Maule Dataset 46
5.3 Data Representation for CMJ and Workflow on Personalized Dataset 47
5.4 Bland-Altman Charts for Dataset Personalized 48
5.5 Continuous Wavelet Transform with different coefficients for IC Detection 50
5.6 1st and 2nd CWT for Gait Stages Detection in walk 50
5.7 1st and 2nd CWT for Gait Stages Detection in Run 50
5.8 CWT Gait Stages Detection in Transition 52
5.9 Step Detection with Filtered Magnitude Acceleration in Walk 52
5.10 Step Detection with Filtered Magnitude Acceleration in Run 52
5.11 Bland-Altman Charts for Dataset Korea 53
5.12 Bland-Altman Charts for Dataset Hasso 54
5.13 Walk and Jump Sequence with Jump Detection 55

List of Tables

3.1 Classification of Smart Garments according to their performance function 15
3.2 Various smart textile-based ECG monitoring products available in the market or in the development stage 16
3.3 Load calculation algorithm for different devices for sports metrics with the company and units of measure 25
3.4 Load calculation for different devices for sports metrics 27
3.5 Maximum Heart Rate calculations based on age 28
3.6 Intensity cardiac/VO_{2max} zones for different devices and societies for sports metrics 28

4.1 Equations for vertical Jump Power calculation and Force Generated 34

5.1 Results for Maximum Height Vertical Jump for Dataset Maule 45
5.2 Results for Maximum Height Vertical Jump for Dataset Personalized 45
5.3 Mean Velocity Difference between Two Step CWT - Treadmill 54

A.1 IMU Plux Specifications 73
A.2 IMU Plux Biosignals Operating Ranges 73
A.3 IMU MPU-9250 Operating Ranges 73
A.4 IMU Physilog®5 Operating Ranges 74

Abbreviations and Symbols

API	Application Programming Interface
CMJ	Counter Movement Jump
CWT	Continuous Wavelet Transformation
ECG	Electrocardiogram
EE	Energy expenditure
E-Textile	Electronic Textile
GPS	Global Positioning System
HAR	Human Activity Recognition
IC	Initial Contact
IMU	Inertial Measurement Unit
MEMS	Micro-electromechanical System
TO	Toe Off
UWB	Ultra Wide Band
VJ	Vertical Jump

Chapter 1

Introduction

1.1 Context and Motivation

The history of humanity has always been intertwined with the practice of sports. It is an ancient activity, with records of Olympic sporting events dating back seven hundred years before Christ. Despite these recorded dates, it is possible that such events were held even earlier. This underscores the historical significance of sports for human civilisation. Since the inception of these competitions, the selection and training of the best individuals for specific tasks have been integral. Training has focused on enhancing physical attributes like strength, flexibility, and speed and refining techniques for various movements and actions. Traditionally, the assessment of these training regimens relied on empirical experience gained in different disciplines. Today, the advancement of statistics and technologies such as wearable devices allows athletes and coaches to access real-time, uninterrupted, quantifiable metrics of training sessions. This enables analysis and the derivation of historical improvement rates for planned workouts.

This work arises from the motivation to accompany and improve the sports activities performed by users during training sessions, providing real-time information that allows the quantification and evaluation of the performance of athletes. This work is integrated within the TexP@ct project and has particular motivation in the search for innovation and digital improvement of the textile industry in Portugal. The project will focus on a teenage audience and on developing useful metrics within physical education classroom settings.

1.2 Objectives

This dissertation's objective is to create algorithms for obtaining metrics that allow the quantitative evaluation of a sports session for physical education classrooms from information provided by inertial measurement units (IMU). As its name indicates, the IMU device will provide inertial information about the centre of mass of the subject who will wear the device. From this information, it will be possible to characterise the movements of the centre of mass performed by the individual during the training session. This characterisation may vary depending on the modality

and exercise the user performs. The metrics that will be given focus will be the maximum height obtained in the case of vertical jump and the speed for walking and running. These provide sufficient information for the load of the lower limbs and are a quantitative method of progression in the exercises performed.

This work seeks to develop an easy-to-use tool to evaluate the performance of athletes based on information provided by an IMU. In addition to assessing the performance of the athletes, these tools will provide feedback on the improvements and progress that can be made over time. Also, it will give the coaches a tool for managing the workload of athletes to avoid overload injuries.

1.3 Document Structure

This work reviews the most critical current metrics when evaluating the performance of a sports session. Also, the ways of calculating them and the devices used to extract information for qualitative and quantitative metrics evaluation. The bibliographic review highlights the methods used to obtain information from each device and how they can present the information. An investigation was also carried out on the devices currently on the market that perform similar tasks for specific sports or sports activities in general. The general topic of wearables, smart textiles, and garments was addressed. The research also consisted of a review of the state-of-the-art algorithms used by the devices, such as artificial intelligence, for extracting information for the prediction and evaluation of training sessions. This review included the current methodologies used to evaluate each algorithm and their comparison as some previously validated strategies were made.

The document is structured in five chapters. The first is the introductory part of the dissertation. The second chapter refers to the theoretical concepts and the explanation of the devices that will be used to obtain signals; in this case, there will be a description of the inertial motion units and the information extracted from an electrocardiogram. A technical review of these concepts and how these devices usually provide the information are made together. In addition, in the case of inertial units, orientation is emphasised due to its importance at the time of extracting the associated metrics. The section also includes concepts of positioning algorithms such as global positioning systems (GPS), even though they will not be initially considered for the project due to their importance as a validation method. In the description of electrocardiography, all the variables that can be extracted for medical and sports cases are included, emphasising the latter. The workflow by which the characteristics are extracted is also presented, mainly referring to the post-processing of the electrodes.

The next chapter reviews the state-of-the-art; a complete review of wearables and garments in general is made. The idea is that the device can be integrated into sports clothing at the time of the session. Within this, a more specific review of sports vests with integrated GPS is made due to the similarity in the metrics extracted by parts of these devices. Next, a bibliographic review of the methods of sports movement recognition is made based on bibliographies of human activity recognition. In this, algorithms based on machine learning, such as extracting physical parameters, are evaluated. Describes the parameters and methods used for the correct classification

of activities. Also explains the methods used to validate these classifications. In addition to motion recognition, these are based on metrics such as speed, distance, jump height, etc. This will allow the athlete and coach to have a quantitative metric of the actions performed at the moment and measure their progression over time. This part also details the methodologies used to validate the quantifying of metrics, which are considered the goal standards and the devices by which the extraction of characteristics is performed. In addition, a bibliographic review of the external and internal load for training regulation is carried out. The external ones are based on accelerometer readings and include a comparison between the different devices and criteria when calculating the external load. Similarly, the algorithms for calculating energy expenditure and the cardiac intensity at which the sessions are performed are presented for the internal load. The fourth chapter describes the methodology of the flow of the algorithms used to extract metrics. It also describes the measurement instruments used and the protocol defined for performing the tests of the dataset generated and used from the web.

The fifth chapter presents the results generated in tables and graphs of the experiments performed. A discussion is generated based on the results obtained, and the phenomena are explained. The sixth chapter presents some recommendations based on the results obtained for future work, not only of the dissertation but primarily based on the context of the TexP@ct project that will continue its realisation.

Chapter 2

Theoretical Concepts

2.1 Inertial Measurement Units

IMUs are electromechanical devices that are the main component of inertial guidance systems. They are relatively small and affordable, allowing them to be installed in smartphones and wearables such as watches and activity bracelets. These units usually obtain various data to combine and provide information for the inertial guidance of the object within the sensor plane. The units obtained come from accelerometers, gyroscopes, and, in some cases, magnetometers due to their small size and the use of mechanical, capacitive, and piezoelectric components. These devices are called Microelectromechanical systems (MEMS) (Hazry et al., 2009; Jarchi et al., 2018).

These devices began in the 19th century with Bohnenberger's Machine. The purpose was to determine the rotational speed of an object. With the passage of time and increasing technology, it was used during the Second World War to launch and guide rockets. However, it was not until the 80s and 90s, with the rise of electronics, that they began to be manufactured in smaller dimensions for other applications. There are also IMUs based on optical sensors that can improve the accuracy. However, everything will depend on the application to select the technology. In the case of its application in sports, it has the advantage over video in that its versatility allows it to be used in any environment and the ability to transmit and process this data in real-time. Remember that image processing usually has a high computational cost, and factors such as background and light tend to affect it. The current size of the devices allows athletes to wear these devices on their bodies without limiting training sessions (Tazartes, 2014; Rana and Mittal, 2021).

2.1.1 Accelerometer

The accelerometer's operation principle is based on Newton's second law, which states that the sum of the forces the object is submerged in equals the relationship between the mass and the acceleration it undergoes. In the case of sensors, the mass is known, and the principle is to detect the force to obtain acceleration. In other words, an indirect measurement is used to get the quantity. The capacity variability is used in two parallel plates and fixed electrodes. Between them is a movable mass attached to a spring, and the force exerted varies the capacitance. This change

generates an electrical signal proportional to the acceleration (Ddafshar, 2014). This principle is performed for each axe with different mechanisms to have the accelerations in three dimensions. In the case of most of these devices, they usually have more than one of these mechanisms per axis to have better accuracy and a better range. That is to say, each one is "calibrated" for the different accelerations that the sensor can be subjected to. The principle of the single moving mass accelerometer with the two plates can be seen in Figure 2.1. This principle of moving mass is widely used as it provides a reasonably accurate reading of the acceleration and is done without a high power consumption.

Among the factors that have to be taken into account in the selection of the device depending on the application are Bandwidth, Sensitivity, Voltage Noise Density, Zero-g voltage, Frequency response, and Dynamic Range (Ddafshar, 2014).

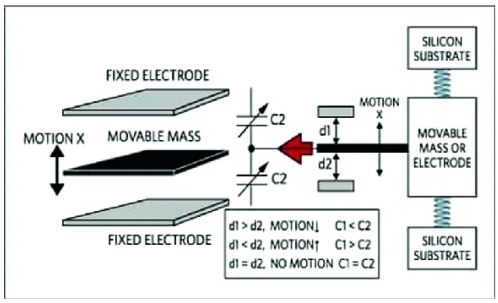


Figure 2.1: Single Moving Mass Accelerator (Ddafshar, 2014)

Accelerometers have several applications today. They vary from the industry for detecting high-speed vibrations of engines or, in the case of sports, for quantifying the accelerations performed. In any case, there are three adversities when working with accelerometers. The first is the drift effect generated since obtaining an absolute zero value is complicated. This problem is problematic when the acceleration is integrated to get the velocity. The second is the noise generated by the micro-movements, which, when amplified, can alter the data. In the case of gravity detection, it is the simplest to control since, by utilizing orientations and rotations, the effect of gravity can be annulled. The rest of the problems require quite advanced methods and filters, and even then, the errors are not corrected by one hundred per cent. It is, therefore, widespread in cases where accelerometers are used for motion quantification to calibrate these elements (Jarchi et al., 2018).

2.1.2 Gyroscope

Gyroscopes provide the angular velocity concerning the sensor frame. The principle of operation is very similar to the one explained for the accelerometers. Still, in this case, the mass is connected to the substrate by springs at 90 degrees relative to the resonating motion as described in Figure 2.2. Classical mechanical principles are used in rotating objects, such as the torques generated by the centrifugal force and joint inertial and Coriolis forces. Relationship obtained from the conservation of angular momentum. It is through these that the angular velocity can be obtained

for each of the axes. Like the accelerometer, the gyroscope presents an arrangement of three models for its representation in the three dimensions (Usubamatov et al., 2018).

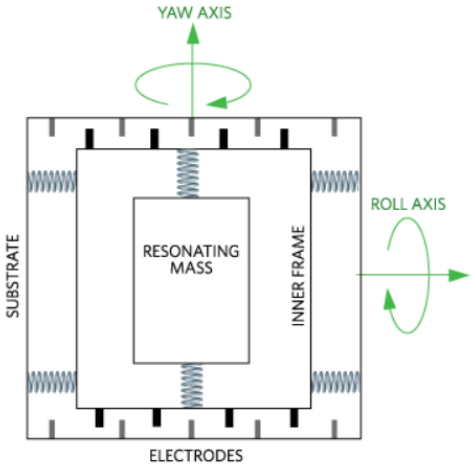


Figure 2.2: Gyroscope Internal Structure (Ddafshar, 2014)

2.1.3 Magnetometer

Magnetometers provide information related to the magnetic feel associated with the sensor, and information supplied by the IMU magnetometer is based on references from the Earth's magnetic field. This is used to detect the device's orientation, especially on smartphones in one of today's applications. Magnetometers have the same principle as induction sensors, based on Faraday's Law. This claims that the magnetic field variation in a defined limited surface generates a voltage. The principle is widely used in this sensor. Still, the detection mechanism can vary depending on technology, one of the most used in the current induction to detect the changes in the magnetic field, as shown in Figure 2.3. The magnetometer's information is displayed in three dimensions related to the three different sensor's axis. Early IMUs did not include a magnetometer, but nowadays, with the growth in technology, it is widespread because it helps to correct the error and orientation derived from the sensor fusion algorithms generated with the gyroscope and accelerometer information (Coillot and Leroy, 2012; Brunner et al., 2015).

2.2 Movement Representations

In engineering, a rigid body refers to an object with a specific shape that remains unalterable in size and form. Based on this definition, different types of object movements can be studied, and that is a concept involved in the kinematics classification. Despite muscles varying in size when performing extension and flexion movements, The biomechanics of the human body can still be understood by considering it as a collection of rigid body parts. In kinematics, the primary movements encompass rotation and translation, represented as orientation and position, respectively.

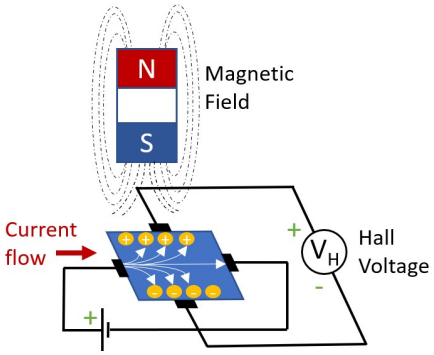


Figure 2.3: Hall Effect Induced with Current on Magnetometer[1]

The specific representation method varies based on the complexity and application of the movement, leading to multiple approaches for representation (Andy Ruina and Rudra Pratap, 2010). The concept of orientation gives the object rotation with respect to a defined frame, which, in this case, could be with respect to earth frame reference from a defined calibrated position. Based on information described in section 2.1.2, the gyroscope gives the rate at which the orientation of the object is changing. There are many mathematical ways to represent the orientation of an object. In the next section, we define these ways and their advantages and limitations concerning each other.

2.2.1 Euler Angles

Euler angles consist of three different angles you can use to describe the rotation of an object in a 3D space. These three angles are commonly named yaw, pitch, and roll. These angles are represented in the Figure 2.4 where each angle represents an axis of the 3D space. This representation is very intuitive to make visual representation, which is one of the many reasons is often used in unmanned aerial vehicles UAVs (drones), and also on airplanes to indicate the altitude, direction, and orientation of a plane.

The problem with this representation is when you are trying to perform inverse kinematics, the process of obtaining the orientation angles based on the physical disposition of the object in the space. This phenomenon is called gimbal lock, which occurs when two axes align, provoking the loss of one degree of freedom, limiting the representation only to a two-dimensional space (Baranek, 2012).

The matrix represented in R_x, R_y and R_z is the transformation matrix for the orientations based on the three-dimensional space generally used in x, y, and z. The orientation can be easily calculated when trigonometry and projected planes are used.

$$R_x(\phi) = \begin{bmatrix} 1 & 0 & 0 \\ 1 & cos\phi & sin\phi \\ 1 & -sin\phi & cos\phi \end{bmatrix} \tag{2.1}$$

[1] https://www.hprobe.com/sensor-test/

$$R_y(\theta) = \begin{bmatrix} cos\theta & 0 & -sin\theta \\ 0 & 1 & 0 \\ sin\theta & 0 & cos\theta \end{bmatrix} \tag{2.2}$$

$$R_z(\psi) = \begin{bmatrix} cos\psi & sin\psi & 0 \\ -sin\psi & cos\psi & 0 \\ 0 & 0 & 1 \end{bmatrix} \tag{2.3}$$

where ψ is known as yaw, θ as pitch and ϕ as roll.

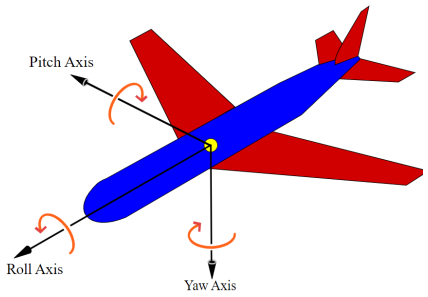


Figure 2.4: Airplane Orientation using Euler Angles

2.2.2 Quaternion

Quaternions are a different way to represent the orientation of the object. This consists of a four-dimension representation, in which one is considered the real part (q_0), and the other dimensions are the imaginary numbers in i, j, and k, respectively. The representation of quaternions can be seen in equation 2.4. The quaternions are very helpful in cases where the gimbal lock needs to be avoided to keep the three degrees of freedom. Another common reason to use quaternions is when combined with sensor fusion algorithms, such as the Kalman filter, to obtain a more "precise" orientation. Operations between quaternions have properties similar to vectors. Since this one does not present commutativity in the multiplication, the result from $q1 \times q2$ is not the same as $q2 \times q1$. Contrary to Euler angles, quaternions are not intuitive due to the incremental dimension and the addition of three imaginary components that do not represent the traditional three-dimensional angle. Also, compared to Euler Angles, the complexity calculation is increased, something to take into account where high frequencies and fast calculations are needed for the hardware to obtain the data (Gordon, 2021).

$$q = q_0 + q_1 i + q_2 j + q_3 k \tag{2.4}$$

The representation of the rotation in the three-dimensional space based on the quaternions representation can be found by the unit vector identified as e_x,e_y and e_z with the respective angles

from that axis θ (Sarabandi and Thomas, 2019).

$$q = \begin{bmatrix} q_0 \\ q_1 \\ q_2 \\ q_3 \end{bmatrix} = \begin{bmatrix} cos(\theta/2) \\ e_x sin(\theta/2) \\ e_y sin(\theta/2) \\ e_z sin(\theta/2) \end{bmatrix} \tag{2.5}$$

2.2.3 Axis Angle Representation

This representation is based on a unitary vector r and a scalar angle θ. The axis r represents a 3D vector with a reference from the World frame, and this arbitrary axis provides information about orientation and rotation according to the rotation matrix. The three components of the unitary vector are orthonormal between each other and follow the right-handedness rule to determine positive directions. It is common for one of the axes of the unitary vector to be aligned with a known or world frame axis to facilitate future calculation and interpretations; this can be visualized in Figure 2.5 (Schneider and Eberly, 2003).

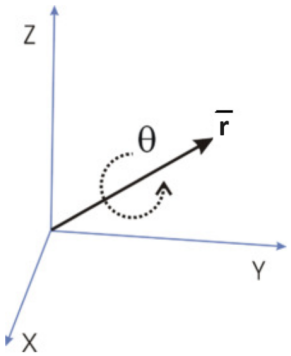


Figure 2.5: Axis Angle Representation

The equation 2.6, also known as Rodrigues' formula, represents the rotation of an object based on the angle axis representation.

$$R(\theta, r) = I + S(r) \times sin(\theta) + S(r)^2 \times (1 - cos(\theta) \tag{2.6}$$

$$S(r) = \begin{bmatrix} 0 & -r_z & r_y \\ r_z & 0 & -r_x \\ -r_y & r_x & 0 \end{bmatrix} \tag{2.7}$$

where r_x, r_y and r_z represent the components of the r arbitrary unit axis vector. θ the rotation angle and I the identity matrix

2.2.4 Rotation Matrix

The rotation matrix representation consists of a three-by-three matrix representation. This represents the rotation for each orientation in a 3-D space. The 3×3 matrix has an orthogonal constraint

that $RR^T = I$ where R^T represents the transpose of the rotation matrix. This helps in the rotation calculation when, based on one orientation, we want to obtain the consequent rotation and vice versa because it is not necessary to calculate the inverse but the transverse of the matrix. The rotation matrix is widely used when we want to calculate the rotation vector, as it gives the transformation of the vector based on the new orientation representation of the object (Hempel et al., 2022). We can obtain the mathematical representation of the rotation matrix based on Euler Angles by equations 2.8 and 2.9.

$$R_{Matrix} = R_z(\psi)R_y(\theta)R_x(\phi) \tag{2.8}$$

$$R_{Matrix} = \begin{bmatrix} \sin(\theta)\cos(\psi) & \sin(\psi)\sin(\theta)+\cos(\psi)\sin(\phi) & -\cos(\phi)\sin(\theta)\cos(\psi)+\sin(\phi)\sin(\psi) \\ -\sin(\theta)\cos(\psi) & -\sin(\psi)\sin(\theta)+\cos(\psi)\sin(\phi) & \cos(\phi)\sin(\theta)\cos(\psi)+\sin(\phi)\sin(\psi) \\ \sin(\theta) & -\sin(\psi)\sin(\theta) & \cos(\phi)\cos(\theta) \end{bmatrix} \tag{2.9}$$

2.3 Global Position System

GPS, which stands for Global Position System, and Global Navigation Satellite Systems (GNSS) are systems based on radio navigation that can provide location. The term GNSS is the generic term for all these types of radio navigation satellite-based technologies. Depending on the region, a different type of satellite system will be used, such as GPS for the USA, GLONASS for Russia, Galileo for Europe, or BeiDou for China, to mention a few. The principle by which the location is known is employing wave transmission at the speed of light. Since the position of the satellite emitting the signal is known, and when the device with a GNSS detects it, the time to have transmitted the signal can be obtained. This time, the distance between these two objects is known when related to the speed of light. Due to the geometry of the Earth being a sphere, at least four reference points are needed to obtain a location (Jensen, 2016).

Depending on the satellite system used, the frequencies to transmit the signals may vary, which is a factor to consider when a product is required or can be used in several parts of the world. It is also worth mentioning that this technology provides correct information only in open spaces and with sky visibility. In the case of sports, most GPS can update the position with a frequency of 1 Hz. The high power consumption compared to IMU is something to consider (Hennessy and Jeffreys, 2018).

2.4 Electrocardiogram ECG

The electrocardiogram represents the heart's electrical signals to generate the blood flow. The analysis of these signals is crucial for the diagnosis and treatment of cardiac abnormalities. The study of these signals began in the early twentieth century with the physician Willem Einthoven. However, it was not until 1957 that a procedure and equipment for mobile ECG detection known as Holter monitor was created. Since then, the size of the devices, electrodes, and technology has

been fundamental for creating instruments with greater precision. At the beginning of the twenty-first century, the study of obtaining this signal using wearable devices began (Zhang et al., 2017; Zhu, 2022).

The electrical characteristics obtained by ECG is a signal with a relatively low voltage, usually below 1mV. In addition, the frequency spectrum for these signals is from 0.05Hz to 150Hz. An ECG signal is typically composed of 5 different points (P, Q, R, S, T), which are used to determine the zones: P wave, QRS complex, and T wave, as can be seen in Figure 2.6. The amplitude and the time between periods and signals can help to determine good cardiac function or detect any abnormality (Zhu, 2022).

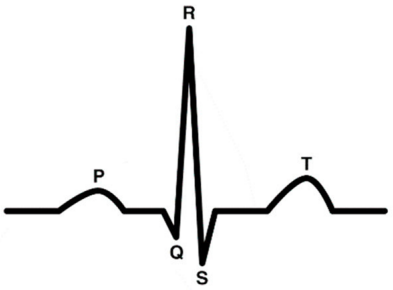


Figure 2.6: ECG signal with (P, Q, R, S, T) points (Zhu, 2022)

The ECG signal acquisition process can be divided into several steps. Signal capture using electrodes, amplification, filtering, and processing for the detection of specific waves or components of the signal.

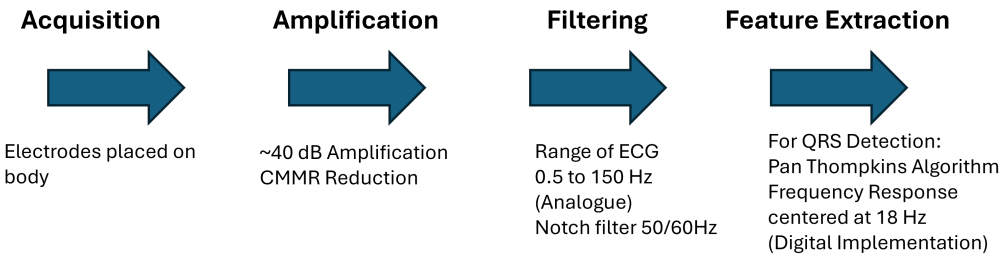


Figure 2.7: Workflow for ECG Acquisition Signal

The signal acquisition may depend on the configuration and the number of electrodes chosen for the desired configuration, but the general process is described in Figure 2.7. At least two electrodes are needed to obtain the voltage difference signal that needs to be amplified. The right leg drive concept is typically used since overall body electrical potential is unknown at any given time. This serves as a reference to the operational amplifier to balance and reference the body's potential (Valchinov et al., 2014; Xia et al., 2018).

The second part is the amplification, but as this amplification comes from a signal difference. Therefore, an amplifier that improves CMMR provides better signal details. Amplifications close to 40 dB are usually used due to the reference values used by the analog-to-digital converters

(ADC). Since most converters today use values between 0 to 5 V or -10 to 10 V (Valchinov et al., 2014; Wangmo et al., 2020).

The third stage consists of filtering the signal concerning its frequency range: a high pass filter at 0.01 Hz and a low pass filter below 150 Hz. In this case, depending on the external power supply, as in most cases, it is necessary to apply a filter at 50Hz or 60Hz, as the case may depend on the country. This filter is called notch filter. For cases where a battery is used as an external power supply the notch filter is not implemented. Also, in the filtering stage, it is essential to consider the filtering that had to be done to avoid aliasing due to the analogue to digital conversion (Valchinov et al., 2014; Wangmo et al., 2020).

The algorithms and data processing part is usually based on implementing digital filters. However, these are based on the nature of the signal or the anomaly they are intended to detect. For example to detect the QRS wave, the range of frequency for this wave is between 10 to 25 Hz. Another approach to detect the QRS wave would be to implement the Pan–Tompkins algorithm. It is also possible to detect each of the P, Q, R, S, and T points mentioned above to process and extract information from them. Cardiac arrhythmia and other anomalies are detected based on the metrics obtained at the points of interest (Castells-Rufas and Carrabina, 2015).

Currently, a twelve-lead method with ten electrodes is used to obtain all the characteristics of the different heart zones. The combination of these signals makes an ECG examination possible nowadays in the medical field. However, most of these procedures are based on the placement of gel electrodes for impedance reduction between the electrode material and the subject's skin. However, for an environment such as sports, the placement of these electrodes and their susceptibility to noise due to muscle activity is one of the complications of using traditional medical methods in wearable devices (Xia et al., 2018). In addition to the required mobility, electrodes placed directly on the skin with gel can cause irritation when measurements are taken over long periods. Also, the reconnecting time and variability of the signal can cause some interruptions. Capacitive-coupled electrodes can be an option to correct this. In the study by Ishida et al. (2007), they evaluated the performance of an ECG signal based on an intelligent textile made of bedclothes with electrodes. The experiment was conducted with the subjects wearing their regular clothes on top, and even the bed sheets could detect the ECG signal from the test subjects. It is essential to mention that the ECG signal acquisition performed better when the subject was stationary. This option could be corrected as was explored in the article by Xia et al. (2018). With a multi-sensor approach (addition of an IMU), they could filter the component derived from the movement in which the electrodes were submitted.

One of the principal advantages of present e-textiles, especially with clothing, is the placement of ECG electrodes in every part of the chest and arms compared to the limitation of the ring or watch. This allows manufacturers to evaluate the performance of different types of electrodes already described and their combination. As the area is more extensive, solutions with combined techniques such as those mentioned in Arquilla et al. (2020) exist. Where a combination of conductive materials such as silver, gold, metal, or conductive ink were evaluated, also, the methods of application of e-textiles are knitting, weaving, sewing, embroidery, etc. This combination was

tested as long with different positions in the chest and abdominal region to obtain conclusions.

2.5 Machine Learning

Human learning is usually referred to as the ability acquired from studies and experiences. Similarly, machine learning refers to the ability of computers to learn from a set of data that the user provides. This consists of a mathematical model where relationships are created so that the machine can predict the output. This prediction can be used for several purposes: recognition, diagnosis, planning, robot control, etc. (Smola and Vishwanathan, 2009). These tasks are usually divided into two different strands, the first one of regression and the second one of classification. There are more, but because of the scope of this work, it was limited to regression and classification.

In the case of regression, the objective is to be able to determine a value in a continuum space to predict. In the case of sports, it can be used for the detection of metrics such as speed or acceleration, the information provided by IMUs or, as mentioned in Szmygin et al. (2023), based on temporal conditions and historical performance, can help to predict the sprint times of an athlete in a hundred meters race. The advantage between traditional methods versus machine learning is evidenced in the latter aspect where you can relate variables that do not have a related model since they only depend on the information, these are often called non-parametric models.

In the case of classification, the algorithm's objective is to correctly determine the class to which the object or input belongs. In the case of sports metrics, it will be fundamental to recognize the actions it is doing, whether it is jumping, running, changing direction, etc. This algorithm is usually trained under databases containing the labels for each sample, making it a supervised algorithm (Gogas, 2022). In the case of not having the labels of the initial classification but only having the information of the characteristics of this and having to perform a grouping, it is called unsupervised algorithms. These are usually grouped in clusters, whose formation methodology may vary (Kotsiantis, 2007). In the case of classification algorithms, there is also usually a classification known as deep learning, which is an algorithm that is based on models that mimic the behaviour of neurons in our brains. Lately, there has been a trend in using these algorithms for their ability in complex models due to their ability to automatically extract features on the internal layers of the model (Gupta, 2021). This is discussed in more detail in the section on biomechanical motion recognition.

Chapter 3

State of the Art Review

3.1 Wearables

Based on the definition, wearables are "electronics which can be used as accessories, embedded on clothes or easy to wear" or with more recently added terms, such as implanted on the body or skin, such as tattoos. These electronics have continued gaining more popularity over the last twenty years. The most popular and well-known wearables are activity monitor wristbands/watches, which allow interaction with other smart devices such as smartphones and obtain and provide information from the subject. Even though sports has been one of the leading markets for wearables, different sectors, such as healthcare and entertainment, have also emerged and are developed for the wearable market (Sanchez et al., 2022).

The first wristband focused on step detection. Nowadays, with the advancements in technology, velocity, heart rate, and oxygen saturation are some of the metrics that can be obtained from this type of device. This has to be done with the advancement in instrumentation and the development of information technology to treat and get benefits from this data. This data collection can be used for many applications regarding sports activities. They can vary to help the coach by providing better training guidance based on quantitative metrics, patterns, and previous records. Besides the coaching guidance, it can give the user/coach with real-time statistics about the performance so the athlete can have an outside quantitative perspective of the results generated in the session. This can result in a major game changer regarding physical exhaust to prevent injuries. Also, fitness tracking based on extracted information can be integrated through big data to form a more systematic and scientific fitness plan, addressing people's different needs (Nan, 2022).

3.2 Smart Textiles

As stated in section 3.1, the definition includes electronics embedded in clothes, which could be called Smart Textile or Smart Fabric, both referring to the combination and fusion of textile and technology. Smart textiles can "sense, react and interact with a range of stimuli conditions and respond to perform a task in a manual pre-programmed manner" (Meena et al., 2023). The

response of the clothing can be based on the environment. Modifying the conduction properties of the fabric by different temperatures, humidity, light or contact with some objects. These changes in the conduction properties can help quantify these interactions to process the information.

E-Textiles can be classified in several ways; one of the most common is based on their performance function as represented in table 3.1. The passive refers to the stimulus generated by the object or the environment and its reaction to it, and the active incorporates not only the sensing but a "trigger" response for the stimulant acting as an actuator, and the ultra-smart textile acts as the active smart textile but with an inner characteristic to reacting and adapting to the stimulus. One example of this last one can be the thermal clothing for harsh conditions where the fabric reacts to the temperature to keep the body isolated and warm reacting based on the temperature sensing outside the jacket (Meena et al., 2023; Sanchez et al., 2022).

Type of Smart textile	**Mechanism in relation with stimuli**
Passive smart textile	sensing
Active smart textile	sensing and responding
Ultra-smart textile	sensing, responding and adapting

Table 3.1: Classification of Smart Garments according to their performance function (Sikka et al., 2023)

Smart textiles have great advantages over other wearables. For example, large parts can be fabricated to benefit signal acquisition, and a mixture of various types of sensors can be incorporated. Also, because the clothing is usually in direct contact with the person using it, bio-information can be obtained as close to the source as possible. Since it can be placed almost anywhere on the body without limiting its extraction to defined parts. Of course, not everything is advantageous since the main restrictions are the duration of the properties due to washing. Since the clothes need to be washed, their properties must remain intact. Washing also affects the electrical properties of information transmission. Many of these fabrics have printed circuits inside or use conductive wires for the transfer of information. However, cleaning products and long-term exposure to water remain two of the main limitations of this type of fabric. Currently, these fabrics have several applications in different industries, as well as the rest of wearables. Most of the applications are focused on sports, healthcare, and entertainment, including the fashion sector. Among the fashion applications is the use of materials with memory, which are currently being worked on to avoid wrinkles in clothing and return to their original state in the presence of a stimulus. In the case of sports and healthcare, it is very common to use shirts to obtain electrocardiograms. In the case of healthcare, it has been used for monitoring patients who have suffered cardiac accidents and require special attention. In the case of athletes, it is used to prevent possible heart failure and to know the details of the effort made by the athlete during training sessions (Lo et al., 2018). The prototypes for ECG smart textiles which had/are been developed nowadays can be seen in table 3.2.

Brand Name	Function
Kymira heart monitoring t-shirt	Detection of the risk of heart attack in athletes and alarming the same on mobile using Bluetooth
Xiaomi Mijia smart t-shirt	Monitoring of physical state of the patient and changes color in case of abnormal heart rate
Sensoria smart socks	Smart socks which count footsteps, calories burnt, altitude & tracking distance.
Emglare smart shirt	ECG & heart rate monitoring system connected to mobile app
AiQ Smart clothing	Five type of electrodes suitable for various applications
HealthWatch ECG t-shirt	ECG monitoring t-shirts allowing remote access to doctors
Sensoria fitness smart t-shirt	Monitor heart rate and store the data in mobile applications

Table 3.2: Various smart textile-based ECG monitoring products available in the market or in the development stage (Sikka et al., 2023)

3.3 Outdoor and Indoor Tracking Vests

The increase in technology allows real-time metrics detection without interrupting the activity. Tracking and metrics detection vests have become part of the sports professions, especially soccer. These technologies may vary depending on whether the sport is practised outdoors or indoors. In most of these vests, one of their main qualities is the localisation of the individual. Most of them use GPS for detection, but if the activity takes place indoors, it is necessary to use Ultra Wide Band (UWB) antennas to locate the athlete. In addition to the location on the field, it is essential to acquire the local position measurements, which track the player's body movements and acceleration. IMUs often extract this information with the combination of artificial intelligence methods to obtain more advanced metrics (Fernández-Galván et al., 2022; Almulla et al., 2020).

There are several outdoor devices on the market today, but the ones that stand out the most are Apex from StatSports[1] and S5 from Catapult[2]. Both are activity monitors with a sampling frequency of 10Hz in conjunction with data processing algorithms and filters for the raw information provided by the GPS. In the case of indoor locations, the best known is the American manufacturer WIMU from HUDL[3]. Like other GPS products, it provides tracking in indoor sports with the help of UWB technology by using a set of antennas for detection in a particular area (Compton et al., 2018; Crang et al., 2022; Rico-González et al., 2022).

In both technologies, vests are combined with specialised software to present metrics in real-time and post-training. The timing of the information varies depending on the product selected. In the case of both technologies, the vest is only a way to secure the device to the athlete's body so that the information obtained by the system is that of the athlete. Currently, some of these

[1] https://eu.shop.statsports.com/products/apex-athlete-series
[2] https://www.catapult.com/solutions/vector-pro
[3] https://www.hudl.com/en-gb/products/wimu

companies use a mixture of this information with video analysis to validate the measurements and generate even more advanced metrics. Figure 3.1 displays the wearable vest with the device and an example of a dashboard generated by this technology.

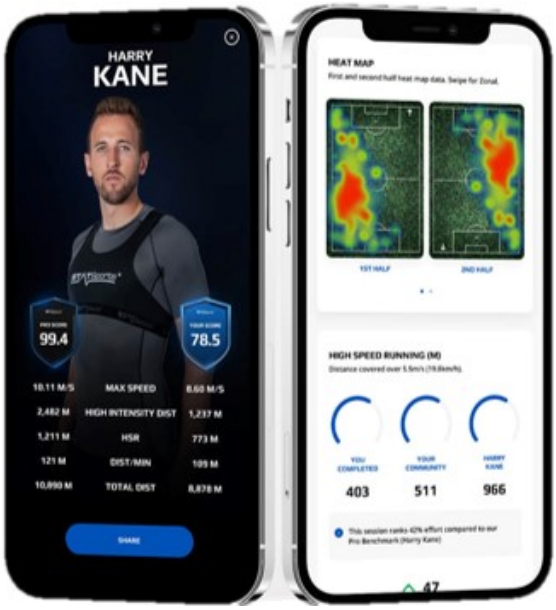


Figure 3.1: StatSports Apex Athlete Series Vest [4]

3.4 Metrics from Sports-Science Perspective

Different evaluation metrics for athletes may vary depending on the age or modality of the person performing the activities. Among these, we can highlight the metrics of locomotion activities, strength, and those related to the sport modality to be performed, such as movement in specific field areas to identify particular skills. This set of metrics provides the athlete with an objective vision of the training in the search for progress in the sports activity.

Locomotion activity metrics refer to activities dependent on or generated from a displacement. Depending on the nature of the activity, whether performed in open or closed spaces, the method of obtaining the location may vary. Mainly, they are used for open spaces for sports such as soccer, football, or rugby (Cummins et al., 2013). Among the metrics we can highlight are distance travelled and speed. It is worth noting that depending on the activity and sport to be performed, these variables may be of interest, as well as the moments and areas in which they are developed. For example, in the case of soccer, it is usually differentiated between the moment in which the athlete is driving the ball and the moment in which he is defending; also, in the case of rugby, which, depending on the zone, can be more valuable in analysis.

GPS usually obtains both speed and distance in open spaces. To have a better relation between distance and actual speeds, it is generally obtained at a frequency of 10 Hz. Since studies have

[4] https://statsports.com/apex-athlete-series

been conducted with frequencies below 10 Hz where the standard deviation for obtaining the distance increased by more than 20% with respect to the frequency of 10 Hz (Varley et al., 2012). These cases usually generate more inconvenience when performing fast movements and short duration, for these cases the information is generally used employing IMU. This not only allows for obtaining these high speeds in short periods but also for other metrics of high importance, such as changes in direction and acceleration. Similar to distance and speed, the location and time in which these actions are performed are aspects to be considered while collecting information.

In the case of strength metrics, we can characterise the force generated during the different training sessions. It can be commonly highlighted that jump strength and power are obtained. It is widespread for evaluating the counter-jump practice for assessing the force generated by the lower limbs at the time of the jump (Toft Nielsen et al., 2019). This activity is usually obtained through force plates; however, due to its limitation to controlled spaces and the inability to evaluate other types of jumps, accelerometers have been used to recognise the jump and quantify these variables.

Now, in the case of the specific metrics of each sport, the characteristics and the way of extracting the information may vary. It is well known, for example, in tennis, the importance of the serve, the mechanics developed, and the acceleration generated in the racquet during this moment. Within the same sport, it is possible to analyse the wrist rotation performed during the different slice strokes (Hadžić et al., 2021). There are several examples for each specific sport, but the scope of this work would be limited to general movements performed during training sessions.

3.5 Biomechanical Movements

Within the literature reviewed, there are two main problems when extracting information metrics from the training session. These would be identifying the activity and its characterisation, i.e., extracting the information. For example, in the case of a soccer player, it may be interesting to describe a sprint's performance. First, it is necessary to recognise the action being performed, "sprint" (an activity that we will describe as biomechanical movement performed); it is essential to identify it from a jump, stretch, or some other movement to obtain the information to be extracted. Then, we may be interested in the characteristics of this movement, such as maximum speed, distance travelled, and duration, to mention a few. These we will call biomechanical movement characterisation. Next, we will provide a detailed review of the state of the art for these two activities, from the devices used to obtain them to the primary metrics used. Also, as mentioned in the introduction, we will emphasise the methods used for comparison with previously validated techniques for analysing the biomechanical movements.

The recognition of biomechanical movements is based on the concept of human activity recognition (HAR), which has become one of the most exciting topics in artificial intelligence. Among the main methods of obtaining and recognising these are pose estimation (computer vision) through cameras based on sensors, usually wearables, and radio frequency signals. This chapter will limit itself to describing the state of the art for wearable sensor technologies. However, the other two methods are often used as comparison methods for evaluation purposes. In

Tina et al. (2021), they compare the input information, the segments to compare, the extraction and selection of features, the classification of the data, and the activation of the classification. For this document, the comparison will be limited to the input information, the features, the models, the classification, and the databases used for training and validation of the methods. While most classifications are based on artificial intelligence models for cases where the identification process differs, they will be mentioned and described.

Han et al. (2022) decided to use the parameters such as acceleration, gyroscope, and magnetometer data provided by the devices with a Deep learning model. In this case, they demonstrated that for each of the activities and databases, the algorithm performs better with the heterogeneous convolution without increasing the number of floating operations for the calculation of the prediction, even reaching values above 99% of recognition of the activities. In addition, a comparison with the results of traditional machine learning methods such as SVM, KNN, HMM, or Forrest Tree is also presented with values of recognition slightly below 99% by the CNN model. Unlike deep learning methods, these methods require manually extracting features, including the mean, variance, standard deviation, max, min, amplitude, kurtosis, and skew of the parameters provided by the IMUs (acceleration, angular velocity, and magnetic fields). This difference can be appreciated in the workflow for classification provided in figures 3.2 and 3.3. They usually adapt the parameters into fixed or variable time windows depending on the activities to be recognised (Bulling et al., 2014; Sazonov et al., 2011; Khokhlov et al., 2018; Brage et al., 2005). The case of sports-related specific cases such as recognition of basketball activities or weightlifting orientations in the forms of Euler angles were included in the model (Velloso et al., 2013).

Han et al. (2022) highlights the comparison with five different databases (OPPORTUNITY, PAMAP2, UCI-HAR, USC-HAD, and the Weakly Labeled HAR dataset). The number of sensors, positions, quantity, and activities to be recognised vary among these. However, for all the methods, the implementation of the heterogeneous convolution presents better results. Although we can reach the same conclusion that the methods cannot be generalised, the advantage is that they can be adapted to any deep learning model, just like a plug-in block. This is especially helpful when comparing sensors that may be captured at various rates to recognise activities with varying time scales. Han et al. (2022) decided to add this modification as a down-sampling parameter. For example, a jump may take 1 to 2 seconds, while walking may take more than 5 seconds. There is no fixed time ratio determined. This concept was introduced by Haresamudram et al. (2021) as the idea of constrastive predictive coding (CPC). It is of particular interest when training a database where there are transition spaces that are not identified and correctly labelled (unsupervised learning) and for speech recognition (Kharitonov et al., 2021; Sutskever et al., 2014; Oord et al., 2019). Another advantage that deep learning methods can present is the interpretation of the data in the time domain. Traditional methods depend on the time windows in which this information can be extracted and the predictions made. However, there is a model called Long-Short Term Memory (LSTM), which, as its name indicates, can consider timing information (Mekruksavanich et al., 2022; Devanne et al., 2019). Like the CPC concept, it helps classify activities with different time durations. This model is based on the fact that they have stored memory cells with variable dura-

tion and retention, and this will depend on the inputs and feedback you can have from the system (DiPietro and Hager, 2020). "This mechanism allows the exploitation of a dynamically changing environmental window over the input sequence history. These mechanisms are performed through structures called gates (Gonçalves, 2021).

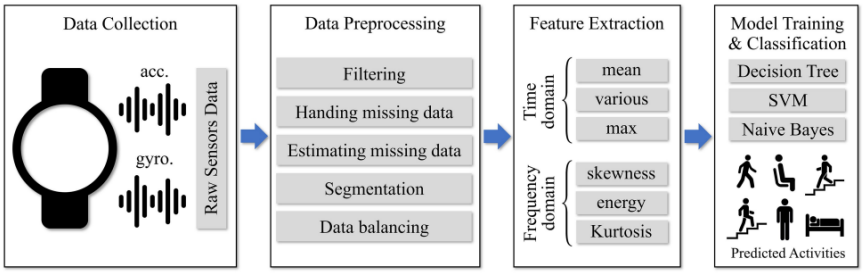


Figure 3.2: Work Flow for Activity Recognition using Traditional Machine Learning Approach (Mekruksavanich et al., 2020)

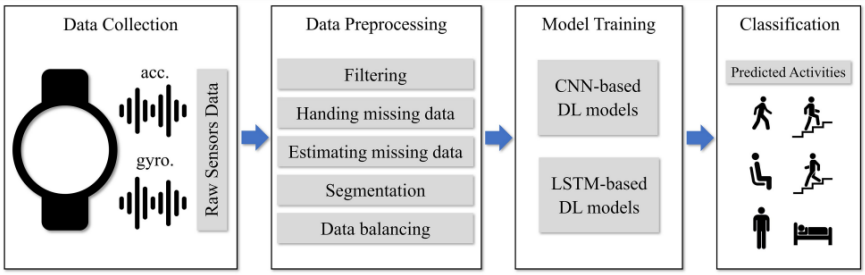


Figure 3.3: Work Flow for Activity Recognition using Deep Learning Machine Learning Approach (Mekruksavanich et al., 2020)

Other methods for recognising activities, such as sitting, walking, or running, can also help characterise movement. The simplest ones can be performed with a fixed or variable boundary delimitation (threshold) as mentioned by Kan and Chen (2012). This is usually based on activity detection and can be used for activity and rest time recognition. In the case of a variable limit, this can be adjusted, and then a binary classification can be performed, which can be complemented by machine learning methods. The threshold value can also be combined with parameters such as body orientation. For example, in the case of jump identification, the vertical acceleration of the jump is explicitly considered for recognising the jump. Employing the threshold, which is usually variable between 1/2 of the weight up to the total weight, using the detection on the vertical axis (Monnet et al., 2014; Miranda-Oliveira et al., 2022; Castagna et al., 2013).

However, when recognising running over long periods, recognising only by threshold could not derive the best results. That is why there are alternatives based on analysing the gait cycle and extracting spatio-temporal parameters (step and stride length, step and stride time, cadence, speed). How the parameters are identified varies depending on the location of the IMU. Among these, the positioning of the foot/ankle area stands out. This allows for the application of a zero update to the gait parameters every time the foot comes in contact with the ground since, at this moment,

its instantaneous speed is zero. In addition, the positioning of these sensors allows obtaining orientation angles for the characterisation of the gait cycle and recognition of walking or running (Benson et al., 2018a; Mason et al., 2023; Kiljander et al., 2021; Terrier and Dériaz, 2011; Young et al., 2022).

Another similar analysis to recognise walking/running when the IMU device is in the waist or chest area is by zero crossing combined with peak detection. This is based exclusively on the acceleration in the direction of motion, i.e., horizontal acceleration on the plane. The information is processed through a fourth-order bandpass filter. A superposition between the original signal and the filtered one is performed, and the local maximum and minimum points are evaluated for the correct extraction of the cycle signal (Terrier and Dériaz, 2011). In the case of having it, the step and the time it lasts are recognised, and it is possible to recognise that the subject is walking/running (Benson et al., 2018a; Kiljander et al., 2021; Young et al., 2022).

Suppose the recognition of walking and running is based on the detection of the gait cycle parameters. In that case, this periodic signal is the same for both activities, varying the speed at which it is performed. Traditionally, the concept of transition from walking to running is given when the support is no longer performed with both feet simultaneously. This means when walking, at least one foot is always in contact with the ground, while when running, there is a period when both feet are off the ground. This transition is said to be the body's natural form of energy conservation, and several studies have been conducted to obtain a limiting speed value at which this transition occurs. Although there is a limiting value, several studies report results close to 2 m/s (Heglund and Taylor, 1988; Thorstensson and Roberthson, 1987). Therefore, one of the methods used for the classification between running and walking from the gait metrics can be from the calculation of speed and whether this is above this limit. When the person is walking fast or running slow, there may be some interpolation of results (Lee et al., 2015).

3.6 Characterization of Movements

3.6.1 Describing Walking and Running through Velocity and Distance

The characterisation of biomechanical movements is generated from quantitative metrics obtained during the movement's performance. In the case of walking or running, movements are usually described by the same metrics, either speed, acceleration, number of steps, distance travelled, or, in the case of more specific metrics, the variation in the stride and the contact force that is derived in the foot and usually absorbed by the tibia (Benson et al., 2018b). The information, as discussed in the section 3.5, will depend on the number of sensors and the position to obtain it. In the case of wanting the contact force and stride variability, several studies show the results with the IMUs placed inside the shoe or attached to the athlete's foot (Zrenner et al., 2018; Donahue and Hahn, 2022; Bailey and Harle, 2015). There are several ways to extract each of these variables. However, one of the most studied ones is the extraction of gait cycle characteristics. Metrics can be inferred from the detection of certain stages. By generating a garment for use in the trunk part, algorithms

that have at least one sensor located in the trunk for extracting these features will be evaluated. As the gait cycle is a periodic signal, it can be recognised either employing thresholds within the parameters provided by accelerometers, gyroscopes, magnetometers, or a combination of these in the case of orientation (Benson et al., 2018a; Kiljander et al., 2021; Young et al., 2022). As it is also mentioned in the article from the overlapping of the foot and hip signal, we can recognise the peaks in the vertical acceleration signals and the direction of movement; we can detect the moments of contact of the feet at 25%, and 75% are the moments in which the crossings are obtained by the negative accelerations vertically (Zijlstra and Hof, 2003). The feature extractor for stride can also be obtained from machine learning algorithms discussed in the section 3.5.

The first algorithm uses step recognition and combines it with gender and age statistics so that it uses an average to approximate the distance for each step and obtain both speed and distance travelled (Anwary et al., 2018). A similar approach was also presented by Morio et al. (2019), which combined the subject's height with statistical studies on the step length taken. In that study, the authors adjusted the parameter depending on the frequency of detection since a directly proportional relationship between the speed and the stride we make when running was detected. Other procedures are based on the case of integration to relate acceleration with speed and distance. Most of the articles that use this use numerical integration associated with the data collection rate (Rispens; Moe-Nilssen, 1998). It is worth remembering that these are carried out in short and specific periods to avoid problems with the drift derived from the integration of the signals. There are several formats for drift correction, as mentioned on Lim et al. (2020), which use physical information of the subject in combination with the gait detection's parameters to estimate the model regression and integration error correction. One of the algorithms that uses numeral integration combines a mathematical approach of an inverted pendulum with double support. This model simulates the movement developed by the centre of mass supported by the legs. For this article, the location of the IMU was placed on the back part of the trunk (Zijlstra and Hof, 1997). To avoid the processing of the data and the required knowledge of the gait model, there have been reports of deep learning algorithms that, based on the raw data provided by the IMU, can calculate speed and distance (Zrenner et al., 2018; Hannink et al., 2017).

Motion capture equipment is usually used to validate each of these algorithms, which can be with markers or markerless. These are based on controlled places where these cameras are placed and from which the information of speed and distance travelled by each of the segments of the body is obtained (Filippeschi et al., 2017; Terrier and Dériaz, 2011; Zrenner et al., 2018). This is usually considered the goal standard and the most used validation method. In addition, for those who referred to studies in outdoor environments, a GPS is often used to validate the trajectory and speed, especially during long distances and times (Giandolini et al., 2015; Sandmæl and Dalen, 2023; Donahue and Hahn, 2022). In the case of enclosed spaces, another validation method can be the WIMU Motion Capture part that uses antennas and wireless information processing to obtain the metrics (Rico-González et al., 2022). Other studies are based on the physical relationship of the devices where the measurements are made, such as the treadmill where you can control the inclination, speed, and distance travelled and is often used as a method of validation (Terrier and

Dériaz, 2011; Lee et al., 2015; Benson et al., 2018b). If long distances are used and high accuracy is required, a tool that is often repeated in the literature is the measuring wheel.

3.6.2 Describing Jumping through Time, Height, Force and Power

Jumping is vital for sports such as volleyball, basketball, or soccer. However, apart from being a measure of comparison for specific actions involving the performance of a jump, it serves as a metric indicator of the load, work, and power that the body's lower limbs can generate. That is to say; it is an indicator to measure the capacity and progress that an athlete can have for different activities (Su and Feng, 2023).

One of the algorithms for both detection and quantification of the jump from IMU is based on the time of flight (FT), from the moment of departure to the moment of landing of the jump (Monnet et al., 2014; Skazalski et al., 2018; Montoro-Bombú et al., 2022). This algorithm is based on the detection mentioned in section 3.5, which uses the vertical acceleration relative to the ground. Monnet et al. (2014) evaluates different thresholds to validate which one provides a better approximation of the time of flight of the jump. This results in half of the person's weight being the optimal threshold. From the flight time and using the principles of kinematics, it is possible to calculate the maximum height obtained from the equation 3.1, based on the principle that the time of ascent to reach the maximum point is the same as in the descent. This is based on the principle of gravity and excludes air resistance and factors such as the position will be the same as at the start of the jump (Castagna et al., 2013). In other words, if the subject were to fold his legs at the moment of landing, the quantification of the jump would not be correct, as it would appear to have a longer duration. Another algorithm used to avoid assuming the same posture for the landing as for the takeoff is based on detecting the takeoff point and the instantaneous velocity at the moment of the takeoff (TOV). This is based on the integration and the frequency rate at which the accelerometer samples (Castagna et al., 2013) or could be obtained using the kinematics equations where the instantaneous acceleration of the body is used to get the velocity (Monnet et al., 2014; Mascia and Camomilla, 2021). After the initial velocity calculation, kinematic equations and free fall motion governed by gravity are used. The equation for the calculation of the maximum height is in equation 3.2.

$$h_{max} = \frac{g \times FT}{8} \tag{3.1}$$

$$h_{max} = \frac{V_o^2}{2g} \tag{3.2}$$

where g represents the constant gravitational force, FT is the flight time, and h_{max} is the maximum height. V_o represents the initial vertical velocity of the jump.

Another proposed algorithm is similar to the one used in the running moments, which performs a double integration between the moments from step to step. In this case, it varies between the moment from the beginning to the end of the jump and performs the integration in the component of the direction of the movement (Toft Nielsen et al., 2019).

For the case of metrics such as force in the realisation of the jump, the centre of mass information is needed. From the information provided by the accelerometer, it is assumed that this will be provided by the centre of mass (Castagna et al., 2013; Miranda-Oliveira et al., 2022). Combined with the dynamics equations, the force can be obtained based on the subject's mass ratio to the acceleration. Kerns et al. (2023) mention the importance of the position for the sensor near the centre of mass at the moment of the jumps. For the power of the jump, the relationship between the initial velocity at the moment of the trunk flexion and the acceleration at this instant just before the moment of takeoff can be used to obtain the calculation of the maximum power (Mascia and Camomilla, 2021; Runge et al., 2004).

Most jump evaluations use the Squat Jump or Counter Move Jump movements. These provide sufficient information for assessing maximum height, flight time, force, and power generated during the jump (Skazalski et al., 2018; Monnet et al., 2014). They have also been evaluated in a less controlled context, such as during the same training or official games for jump recognition shown in Skazalski et al. (2018). Among the validation methods for the algorithms, the testing standards are usually force platforms and motion capture, especially for parameters such as force and power. Motion capture, force platforms, or the Vertec device are used to determine the maximum height in jumps (Heredia-Jimenez and Orantes-Gonzalez, 2020; Marković et al., 2021). There are also many commercial devices, such as Vert[5], based on the abovementioned algorithms that could serve as references for algorithm evaluation during sessions in playing environments (Borges et al., 2017).

3.7 External and Internal Workloads

The quantification of training loads has evolved in recent years because several studies show the relationship between regulating training volume and reducing the risk of injury (Gómez-Carmona et al., 2020). It is essential to mention that although it provides us with a quantitative parameter, each athlete responds in a personalised way to different exercises and load metrics, which is why it is often used to customise training for each athlete and understand the performance they can achieve (Gómez-Carmona et al., 2019). Within the literature, there is a separation of internal and external loads. The external loads are usually associated with people's movements (locomotion) performed by people and can be quantified through accelerometers (IMU). These are generally in changes of direction, jumps, translations, and rotations (Cabarkapa et al., 2023). Internal loads are usually the physiologic responses from the body reacting to various tests being performed. These are typically obtained through heart rates or oxygen consumption and are generally presented in intensity indexes to characterise these (Cabarkapa et al., 2023).

3.7.1 External Loads

In a study conducted by Gómez-Carmona et al. (2019), a comparison was made of each of the ways to obtain the load for a soccer team training. All load measure algorithms' were highly

[5] https://www.myvert.com/

correlated and presented effective methods to control the load of the players. However, between methods, the result by itself of the load varied due to the difference between the equations and the units of measure for the calculations. Different methods (Rowlands et al., 2014; Reche-Soto et al., 2019; Boyd et al., 2011; Gentles et al., 2018; Dalen et al., 2016; Bowen et al., 2017), are listed in table 3.3 with the formula for each of these. From table 3.3, we can see the algorithms of companies ActiGraph, Zephyr, and ZXY SportTracking use the raw variables obtained from the accelerometers and obtain the norm from them. Then, the scaling factor varies depending on the dimensionality. The other algorithms use the difference of squares between consecutive measurements. However, Boyd et al. (2011) also refers to the importance of the direction in which the movements are made since instead of using the raw information, this needs to be processed to identify the movements in front (anterior-posterior), side, and vertical, to have as inputs the accelerations in each of the directions. In the case of the algorithm developed by RealTrack Systems (Reche-Soto et al., 2019), it shows the intensity calculation at a specific time, and we can also do the summation to find the accumulated load. Skazalski et al. (2018) make an evaluation on another device, Vert, which is exclusive for vertical jumping in both training and game environments and come to the same conclusion as Gómez-Carmona et al. (2019) in which through IMU attached to the body it is possible to obtain the workload and use this amount for the administration and management of the training sessions.

Company	**Formula**	**Units**
ActiGraph LLC & GENEActiv	$\sum \sqrt{(x^2+y^2+z^2)}$	(g's)
RealTrack Systems	$PL_{RT} = \frac{\sqrt{(x_n-x_{n-1})^2+(y_n-y_{n-1})^2+(z_n-z_{n-1})^2}}{100}$	(a.u)
Catapult Sports	$\sum \frac{\sqrt{(fwd_{t=i+1}-fwd_{t=i})^2+(side_{t=i+1}-side_{t=i})^2+(up_{t=i+1}-up_{t=i})^2}}{100}$	(a.u).
Zephyr	$\sum_{s=1}^{n} \frac{\sqrt{(x_s^2+y_s^2+z_s^2)}}{9.81}$	(N/s)
ZXY SportTracking	$\sum_{s=1}^{n} \frac{\sqrt{(x^2+y^2+z^2)}}{800}$	(a.u)
StatSports	$\sum \frac{\sqrt{(aca_{t=i+1}-aca_{t=i})^2+(acl_{t=i+1}-acl_{t=i})^2+(acv_{t=i+1}-acv_{t=i})^2}}{100}$	(a.u)

Table 3.3: Load calculation algorithm for different devices for sports metrics with the company and units of measure

where $x, y, z, x_n, y_n, z_n, x_s, y_s, z_s$ represent the acceleration on the sensor reference frame. Abbreviations $fwd_{i=i-1}, fwd_{i=i}, aca_{t=i-1}, aca_{t=i}$ represent the acceleration in the AP direction for the

previous and actual iteration respectively. $side_{i=i-1}, side_{i=i}, acl_{t=i-1}, acl_{t=i}$ represent the acceleration in the lateral direction for the previous and actual iteration, respectively. Finally abbreviations $up_{i=i-1}, up_{i=i}, acv_{t=i-1}, acv_{t=i}$ represent the acceleration in the vertical direction from the previous and actual iteration respectively.

3.7.2 Internal Loads

One of the variables of interest within the internal metrics is the energy consumption performed by the athlete during the training session. This is usually related to the oxygen consumption during the session (Loshkarova, 2020). This is related to other variables such as sex, age, height, and weight to obtain the relationships and to quantify the energy consumption. However, Lee et al. (2021) makes a comparison from different algorithms between accelerations and heart rate. It determines a better accuracy in the case of algorithms that used heart rate than accelerations, which were represented in table 3.4. In the case of Schmitz et al. (2005) and Lyden et al. (2011), only accelerations from a threshold above 0.033g's were taken into account, and the variable to be entered is the magnitude of accelerations. Besides, for this one, it is necessary to remove gravity so as not to affect the calculation of the internal load. Based on energetic expenditure calculation from accelerometers, Heil (2006) and Crouter et al. (2006) present alternatives for the calculation from steps in a time interval. The algorithms for step detection are the same as those mentioned in section 3.6. However, since it is not a characterisation of the movement, the data acquisition rates of the accelerometers are usually below 50 Hz. Also, Heil (2006) and Crouter et al. (2006) present an alternative that the parameters are based only on the number of steps and do not depend on other physical variables such as sex, age, height, or weight. It is essential to mention that in Loshkarova (2020), there are also differences between the algorithms for energy consumption between athletes and non-athletes, so the amount of physical activity per week may be one of the quantification variables to be taken into account.

In the case of those based on heart rate, there are two options. The one presented by Pettitt et al. (2007) where first from the heart rate, calculates the maximum oxygen consumption from the heart rate and derived from this calculation the energy consumption is obtained. This is based on the calculation of oxygen per heartbeat pulse to make the calculation. In addition, the methodology of obtaining this varies with respect to the others because it uses data at rest and makes the comparison after the physical exercise for the quantification of energy consumption (Pettitt et al., 2007). Another alternative for the case of heart rate is Lee et al. (2021) algorithm based on the linear relationship that can be observed between energy consumption and the increase in the heart rate of the person. The case of Eston et al. (1998) not only makes use of the estimation but also compares it with the accelerometer information to quantify the movement of the centre of mass. The case of Lee et al. (2021) presents the equation for calculating energy consumption with heart rate and physical parameters.

Source Input	Formula
Accelerometer (Step/min)	$EE = 0.01217 + [(5.268E-5) \times steps/min]$ if steps/min ≤ 1200 $EE = 0.02663 + [(1.107E-5) \times steps/min]$ if steps/min > 1200 EE (kcal/min) (Heil, 2006)
Accelerometer (Step/min)	$EE = 1.46 + 0.2107\ln(step/min) - 0.059\ln((step/min)^2) + 0.015\ln((step/min)^3)$ EE= (MET) (Crouter et al., 2006)
Accelerometer (x2 + y2 + z2)	$EE = -1.033 - (0.2 \times [f:0;m:1]) - 0.19 \times age - 0.002 \times ht + 0.117 \times wt + 0.001 \times VM$ EE (kcal/min), $VM = \sqrt{x^2+y^2+z^2}$ Lee et al. (2021)
Heart Rate (beats/min)	$EE = -13.8 - (0.461 \times [f:0;m:1]) + 0.24 \times age + 0.023 \times ht + 0.075 \times wt + 0.069 \times hr$ EE (kcal/min) (Lee et al., 2021)

Table 3.4: Load calculation for different devices for sports metrics

The goal standard for this type of validation is usually metabolic equipment. These are usually a mask placed over the nose and mouth to analyse the moments of inspiration and expiration in the case of sports evaluations (Lee et al., 2021). Also, most methodologies varied depending on the characterisation objectives. Pettitt et al. (2007) performed exercises on the treadmill until reaching the point of maximum heart rate and then made all the measurements at rest. The opposite was the case for Lyden et al. (2011) and Lee et al. (2021), where they performed activity for a specific time and compared it with the resting data for energy consumption.

Intensity is another metric used to describe the internal loads undergone by sports during training sessions. It is usually based on the percentage of maximum heart rate (%HR) associated with the individual or the percentage of maximum heart rate at rest (%HRR). Maximum heart rate is defined through the relationship to age defined in table 3.5 (Zhu et al., 2022). From maximum frequency, it is necessary to have the data of the average frequency of physical activity and the frequency at rest as mentioned by Chen et al. (2022). To give as a result, the model from equation 3.3 for obtaining at rest. The relationship is presented in equation 3.4 for maximum heart rate percentage. In Howley (2001), they present another model based on the VOmax, with other limits, since they have a relationship directly provided between the heart rate and VOMax, as seen for the part of the energetic consumption. Another of the present algorithms (Roy and Mccrory, 2015), apart from the variability of the maximum heart rate associated with age, evaluated the influence of physical activity when comparing professional athletes with sedentary people. Variables that influenced the calculation of maximum frequencies for each subject.

$$\%HRR = \frac{HR_{activity} - HR_{rest}}{HR_{max} - HR_{rest}} \times 100 \tag{3.3}$$

$$\%HR_{max} = \frac{HR_{activity}}{HR_{max}} \times 100 \tag{3.4}$$

$HR_{max} = 220 - age$
$HR_{max} = 226 - age$
$HR_{max} = 208 - 0.7 \cdot age$

Table 3.5: Maximum Heart Rate calculations based on age (Roy and Mccrory (2015)

Five intensity zones are usually identified from the percentages based on the ratios calculated in Equation 2. The intensity zones defined by Howley (2001) are very light, light, moderate, hard, and very hard. Some differences exist between the zone percentage limits and methodologies, which are evidenced in the table 3.5.

Company/ Society	**Metric**	**Very Hard/ Maximum**	**Hard/ Vigorous**	**Moderate**	**Light**	**Very Light**
ACSM Garber et al. (2011)	%HRmax	≥96	77-95	64-76	57-63	<57
ACSM Garber et al. (2011)	%HRR	≥90	60-89	40-59	30-39	<30
ACSM Garber et al. (2011)	%VO2max	≥91	64-90	46-63	37-45	<37
CDC HHS (2008)	%HRmax		77-93	64-76		
FitBit Fitbit LLC (2023)	%HRmax	≥85	70-84	50-69		
Polar Polar Oy (2021)	%HRmax	≥91	80-90	70-80	60-70	50-60
Garmin Garmin Ltd (2019)	%HRmax	≥91	80-90	70-80	60-70	50-60

Table 3.6: Intensity cardiac/VO_{2max} zones for different devices and societies for sports metrics

Chapter 4

Methodology

Different types of datasets were used to validate the developed algorithms, both personalized and developed for similar projects. For each of these, we will describe the capture devices used to collect and process the information. There will also be a description of the methodology carried out, along with the variables to be collected within the experimentation and the objectives for each of the methodologies.

Four datasets were used and will be explained during this chapter, for reference of this chapter and the results, the Dataset generated by the Catholic University of Maule would be referenced as Maule dataset. The dataset generated in conjunction with the faculty of Sports will be called Personalized Dataset. The dataset generated by the Hankyong National University of South Korea will be referenced as the Korea Dataset. Lastly, the dataset generated by the Hasso-Plattner Institute would be referenced as the Hasso dataset.

4.1 Jump

According to what is described in the section 3.6, jumping is characterized by a pronounced acceleration pattern in the vertical axis. Both at the moment of take-off and landing. This section will analyze and describe the Jump based on the maximum height attained. The patterns before the take-off moment described movements corresponding to the impulse necessary to generate the jump. This last characteristic allows the implementation of the initial velocity method. In the case of the time method, the detection of the take-off and landing moments was obtained to make a description of the jump through the flight time. The primary difference between both methods is that flight time assumes the position of take-off is going to be the same as the landing spot. If the subject flexes the knees at the moment of landing, it might interfere with the results calculated. The flexion of the knees is a natural movement that helps to cushion the jumps. In the case of the jump studied, CMJ should not present a flexion at the moment of the landing. Nevertheless, this was not a factor to be considered to discard or not a jump at the moment of the signal acquisitions. The initial velocity method has no restraint for the landing but has increased complexity in determining the initial velocity of the jump.

For both methods, two different databases were used. The first one was collected by the Universidad Católica del Maule, Chile Rico-Garcia et al. (2022). This database consisted of 10 counter-move jumps performed by four healthy individuals between the ages of 20 and 30 years. There was a one-minute rest time between jumps to avoid fatigue. 7 inertial devices were distributed in the lower limbs of their bodies, as shown in Figure 4.1. It should be noted that for our analysis, the information processing was limited to the information provided by the sensor located on the trunk of the subject (sensor #3). The data capture was performed with the IMU MPU-9250[1] (InvenSense, California USA), which has an accelerometer, gyroscope and magnetometer, see Annex 1 for operating ratings. It should be noted that the IMU was integrated with a microcontroller and a Bluetooth module to allow the transmission of information. The data was collected at a frequency of 75 Hz. In addition to the information provided by the IMU, the study conducted at the University of Maule captured the counter jumps with an optical system, Optitrack OPTIHUB2[2] (Natural Point, USA), to make the comparison and use it as ground truth. For this, the optical marker has to be incorporated; their position is described in Figure 4.2. The processing of the information in our case was limited to the marker placed on the trunk. The information collected by this system was generated at a frequency of 100 Hz.

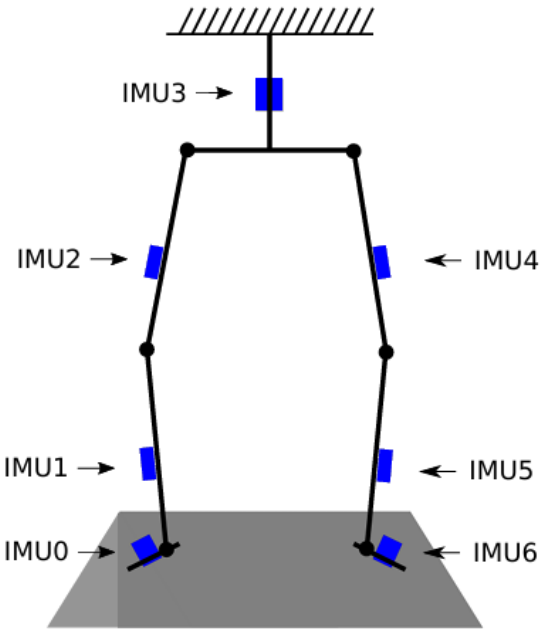


Figure 4.1: Low Limb representation with IMU sensor location for dataset Maule (Rico-Garcia et al., 2022)

For the personalized jumping dataset, the methodology was based on the Maule dataset and was captured with the help of the Faculty of Sports from the University of Porto. However, the sensor position and its properties were modified, as can be seen in Figure 4.3. A single IMU sensor

[1] https://invensense.tdk.com/products/motion-tracking/9-axis/mpu-9250/
[2] https://optitrack.com/accessories/sync-networking/optihub/

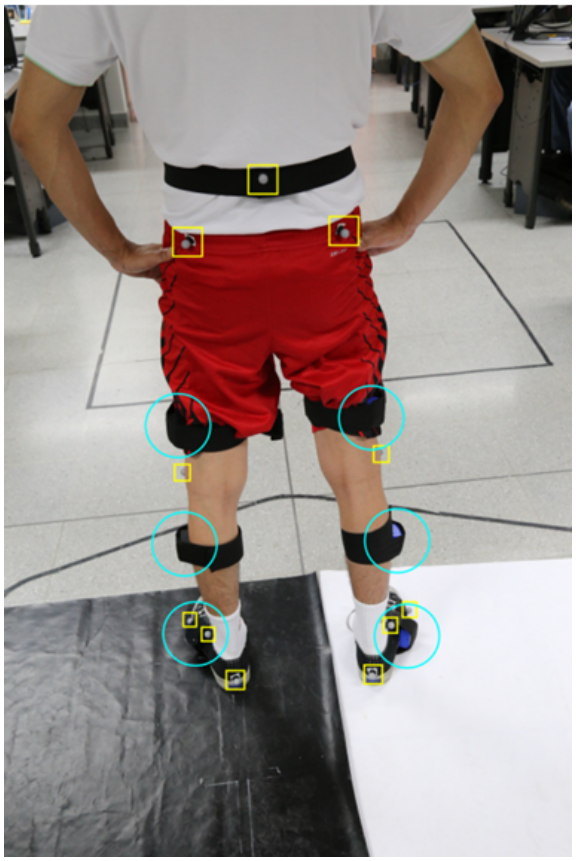


Figure 4.2: Optical markers location for dataset Maule (Rico-Garcia et al., 2022)

was placed near the T8 position of the column. This was based on a previous study conducted by the faculty of sports, which allowed us to determine which position could provide a better reading with a single IMU over the centre of gravity of the subject in question. The sensor is integrated into a central module[3] fabricated by PLUX Biosignals (Lisbon, Portugal), which has an accelerometer and gyroscope, see Annex 1 for operating ratings. This sensor is integrated with a central module that transmits the information via Bluetooth; this will be modified for a WI-FI protocol for the next prototype. This central module is attached by a piece of clothing, generating enough compression to avoid additional movements and only transmit the reaction of the area of interest. The acquisition rate for the accelerometer and the gyroscope was 1000 Hz. For this dataset, the Xsens Awinda Model[4] (Movella, Netherlands) was used as the gold standard comparison. As indicated in Figure 4.4, it has 17 IMU sensors placed in various parts of the body that allow a representation of body movement in each of its main extremities. The 17 Xsens IMUs have an accelerometer, gyroscope and magnetometer information with a sampling frequency of 200 Hz. The data was extracted by the software (Xsens MVN Analyze), but our interest was limited to the pelvis and t8 sections. These points were selected based on the previous set and by proximity to the sensor placed as a reference point. The software allows the segment

[3] https://www.pluxbiosignals.com/collections/wearables-ble/products/muscleban-ble
[4] https://www.movella.com/products/motion-capture/xsens-mvn-awinda

to be localized during data capture. Therefore, we limit ourselves to determining the position at the beginning of the jump and obtain the difference with the maximum value attained, which determines the maximum height reached during the jump. This personalized dataset consisted of a single test subject with a height of 1.83 cm and a weight of 84 kg who performed 10 counter-movement jumps. The time between each jump was 1 minute to give the subject enough time to recover and allow the software to store the information. During data acquisition, the test subject wore the vest and the Xsens suit at the same time. During the data collection, other procedures were performed, such as the calibration of the Xsens system and various other activities. However, for the creation of the jumping dataset, the data acquisition was limited to the counter-movement jump.



Figure 4.3: Worn Vest with the placement of the IMU Sensor on t8 section in calibration position

The processing flow for this dataset can be seen in the image 4.9. The first step consisted of resampling the data. This was because there were variations of ± 2 milliseconds between data samples, i.e. the sampling rate was not constant, and there were also cases where 1, 2 or even 3 samples were missing. Therefore, at the time of data processing, a single sampling was performed, and a linear regression was used to calculate the missing and corrected values. This process was performed to ensure the correct detection of the take-off and landing moments, as well as for the calculation of the time between them and the correct integration of the acceleration vector. The second step was the implementation of a low-pass filter with a cut-off frequency of 20 Hz. The

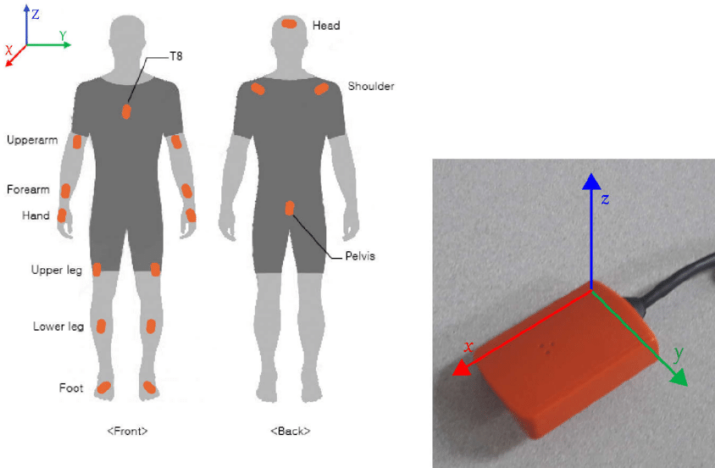


Figure 4.4: XSens Front and Back Location of IMU'S (Jang et al., 2018)

filter design is referenced in several works (Rico-Garcia et al., 2022; Kerns et al., 2023) as the maximum frequency generated by human body movements and to eliminate high-frequency noise disturbances. The generated filter is a fourth-order Butterworth filter, which is applied to each of the accelerometer axes.

The third step was the calculation of the orientation based on the information provided by the IMU. Three different sensor fusion algorithms were implemented: Madgwick, Mahony, and Extended Kalman Filter. Madgwick and Mahony stand out for their agility in mathematical calculations; however, the Kalman filter allows the addition of the magnetometer variable, which usually helps to obtain a more accurate orientation. For the use of these algorithms, the AHRS System module[5] was used, which simplified the method's implementation. However, something to take into account is the reference used by this module and the dimensions used, so depending on the ground reference that the IMU has in the initial calibration, different transformations have to be performed to use the AHRS System module methods. For a correct calibration, it is necessary that the subject remains in a stationary position as in Figure 4.3 for at least the first second of data collection. The fourth step is the removal of gravity. As discussed in chapter 2 the accelerometers are affected by an offset acceleration reading generated by gravity. For motion analysis purposes, it is convenient to remove gravity for data extraction. For this, we need to know the direction of the gravitational vector, which, in the case of the Maule dataset, is towards the negative "z" axis. For the case of the personalized dataset, it is in the direction of the negative "y" axis. This step involves the rotation of the acceleration reading from the sensor frame to the earth's frame based on the orientation. After performing this transformation, the value needs to be subtracted from the gravitational vector of the dataset. To validate the correct removal, the expected value in the vertical axis for the standing position should be zero or close to it.

The fifth stage is based solely on the reading of the vertical acceleration axis, already filtered and gravity removed. By means of upper and lower threshold values, it is possible to detect the

[5] https://ahrs.readthedocs.io/en/latest/index.html

Output Metric	**Method**	**Formula**
Power	Lewis	$P(W) = \sqrt{4.9} \times$ body mass(kg) $\times \sqrt{jumpheight(m)} \times 9.81$
Power	Harman	$P(W) = 21.2 \times jumpheight(cm) + 23 \times bodymass(kg) - 1393$
Power	Johnson	$P(W) = 43.8 \times jumpheight(cm) + 32.7 \times bodymass(kg)$ $-16.8 \times height(cm) + 431$
Force	Newton	$F(N) = bodymass(kg) \times acceleration(m/s^2)$

Table 4.1: Equations for vertical Jump Power calculation and Force Generated

take-off and landing moments of the jump. This is where both methods converge since the flight calculation algorithm uses this detection to calculate the time and uses Equation 3.1 to calculate the maximum height. In the case of the algorithm that uses initial velocity, in addition to the detection of the takeoff time. It uses the detection of the impulse pattern generated just before takeoff to integrate and obtain the velocity at the moment of takeoff, as highlighted in Figure 4.5. After obtaining the initial velocity value calculation, it uses Equation 3.2 to calculate the maximum height attained by the subject.

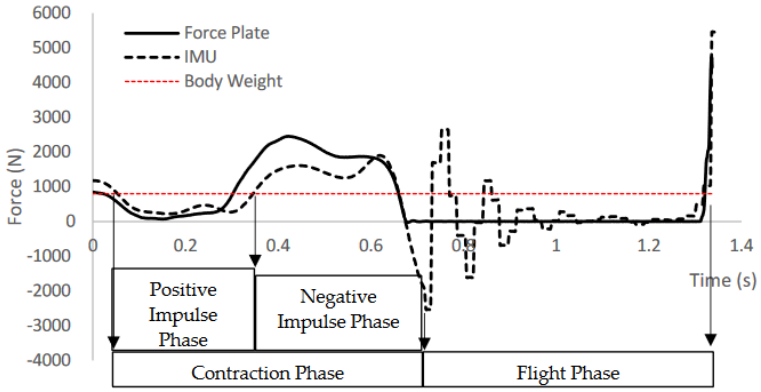


Figure 4.5: Counter Movement Jump Phases with IMU (Miranda-Oliveira et al., 2022)

The last stage was based on the formulas in Table 4.1 to obtain other parameters such as jumping power and generated force. Some of these parameters, in addition to those obtained by IMU, such as flight time or maximum height, are combined with the person's physical parameters, such as mass, to extract the metrics. This part could not be compared due to the lack of a gold standard reference. Therefore, in the Results chapter, we will limit the presentation of the data related to maximum height.

4.2 Running

The same methods used for vertical jumps cannot be applied to lateral movements like walking or running. Because these movements are usually performed repetitively, a simple integration to identify variables such as speed or distance travelled would generate an accumulation of drift that would vary over time in a linear or quadratic way, depending on the metric. Therefore, two

different methods were defined for the calculation of both variables. The first was based on the generation of a pedometer, which refers to the identification of the number of steps taken, and the second method was also based on this recognition in addition to detecting the different stages of the gait cycle to characterize and recognize the stance and swing stages. In the following, we will describe both the methodology used, the database, and the data collection device. Two datasets were used to validate these data, both built in a controlled environment on a treadmill that allowed displacement in a single direction at a speed as constant as possible. The first dataset was generated by the Hankyong National University of South Korea (Lee and Lee, 2024), which consisted of 7 healthy adults (age:24.4 $\pm$ 1.7 years, height:1.73 $\pm$ 0.06 m, weight: 72.8 $\pm$ 6.3 kg) who performed 8 different tests lasting between 8 to 10 minutes each of data collection. All subjects performed 2 flat walks at 4 and 6 km/h, 2 runs at 7.5 and 9 km/h, 2 walks at 4 and 6 km/h with a 3% incline and 2 walks at 4 and 6 km/h with a 6% incline. To ensure consistent data, subjects were asked to rest for at least three minutes before each experiment. The data was collected by 5 IMU Xsens MTw[6] (Movella, Netherlands) modules located as shown in the Figure 4.6. The data collected by IMU was at a sampling rate of 100 Hz and then processed by a fourth-order Butterworth low-pass filter with a cutoff frequency of 6 Hz. For this dataset, the measurement that we will take as a reference is the one indicated by the treadmill so we will make a comparison of the speed obtained. Due to privacy-related issues, the shared data was limited to one subject performing the test at different speeds and inclinations.

The second dataset was generated by the Hasso Plattner Institut with the University of Postdam. This experiment was performed with 15 participants (7 women and 8 men, age:26.4 $\pm$ 3.7, weight: 69.7 $\pm$ 12.1 kg, height: 1.76 $\pm$ 8.8, leg length 86.2 $\pm$ 4.3 cm and PWS 3.9 $\pm$ 0.5 km/h) who had to perform three different tests on the treadmill. First, each participant had to perform a test to select their preferred walking speed. After selecting their preferential speed, the preferential speed minus and plus 20% was calculated to perform the other two trials. The order of the tests for each subject was randomized; each test consisted of the subjects performing the tests for 2 minutes for each velocity. The time between tests was not defined but was required only if the subject needed rest before performing the next test. The data for this data-set was generated by 3 different capture methods. The first employed 7 IMU sensors placed on the subject's feet and trunk as shown in Figure 4.7. The sensor model used was Physilog®5 IMUs[7] (Gait Up, Lausanne, Switzerland). These were configured to obtain measurements at a sampling rate of 128 Hz. In this case, the IMU module can store the information in an SD card since the Bluetooth module was used to synchronize the reading of the 7 sensors. The IMU had an accelerometer and gyroscope only. The second and third capture method was collected by the treadmill itself as it has an OptoGait System and a FDM-THQ pressure distribution system[8] (Zebris Medical GmbH, Isny, Germany). The pressure sensors are located underneath the belt, and the optical sensors are located on the side of the treadmill. Therefore, this dataset can be used to compare both the

[6] https://www.movella.com/products/motion-capture/xsens-mvn-awinda

[7] https://www.gaitup.com/

[8] https://www.zebris.de/fileadmin/Editoren/zebris-PDF/zebris-Prospekte-EN/FDM-T_Prospekt_en_120901_72dpi.pdf

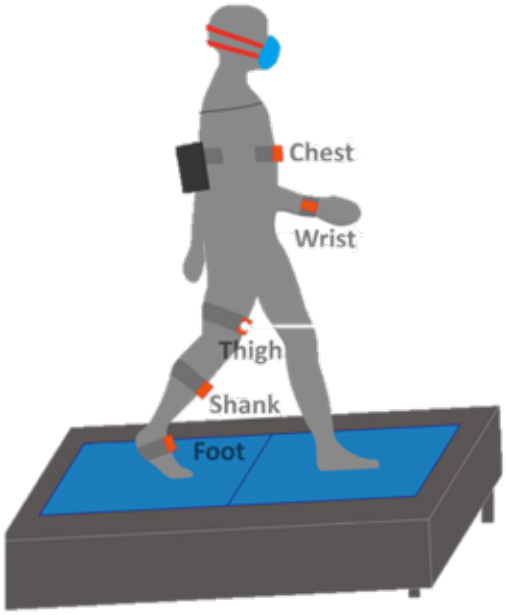


Figure 4.6: Hankyong National University of South Korea Dataset Location for IMU on subject (Lee and Lee, 2024)

speed reached and the distance covered during all or part of the test. However, due to metrics and comparison with the previous dataset, we will focus more on the speed part.

Figure 4.10 represents the flow of the algorithm used for the step detection and the calculation of speed and distance travelled. The first stages are similar to those performed by the vertical calculation. The first step of information processing consisted of the verification and resampling of the data if necessary, to guarantee a constant sampling, in case it was necessary to generate some value, linear regression was used. The second step was omitted in the case of the Korean dataset since the data acquisition was already implemented with a low-pass filter. However, for the Hasso Plattner database, a 2nd order Butterworth low-pass filter with a cutoff frequency of 20 Hz was implemented. The third step consisted of obtaining the orientation. For the rest of the datasets where at least the first second in static stop position was available, the information on this lapse was used for its calibration. The orientation calculation was used to remove gravity and obtain the direction of the body, although in this case, the direction of the accelerometer data used was anterior-posterior (AP).

From the fifth step onwards, the algorithms diverge in a similar way to the vertical jump algorithm. The first algorithm, called step detection, is based on the fact that the acceleration magnitude can represent a gait recognition pattern if the sensor is placed near the centre of mass of the subject. It will not have additional movements as presented in the wrist position (Jarchi et al., 2014). Therefore, the magnitude is processed by a low-pass filter when it is calculated. Since



Figure 4.7: Hasso Plattner Institute Dataset Location for IMU on subject (Trautmann et al., 2021)

the different datasets have different sampling frequencies, it is recommended that the normalized cut-off frequency be at a value of 0.01. In the case presented by Lu et al. (2019), the sampling frequency is 400 Hz, and the normalized value of 0.01 represents a cutoff frequency of 2 Hz. The result obtained is a sinusoidal signal with a vertical displacement centred on a positive value. As it is a repetitive pattern, the detection of maxima through threshold values indicates the step realization for each recognition. In the case of this method, we are not interested in the maximum value attained but in the time difference detected between each of these cases. This time allows us to obtain the cadence of steps performed by the subject in a given time. With the cadence there are two ways to obtain velocity, the simplest is to use the method of inverted pendulum method based on the physical characteristics (leg and subject height) to make an approximation of the distance performed in each of the steps. This can be calculated from the Equation 4.1. The second way would be to opt for the relationship between distance, velocity, and acceleration by integration. Thus, knowing the time between steps, the acceleration component AP is integrated to obtain both the velocity and the distance travelled. To avoid the drift component in this and to obtain a more accurate calculation of each step, Lu et al. (2019) proposes a calibration of steps over a distance of 20m. It is to obtain the signal for a given distance, i.e. at 20m, and then do the signal integration. Compare the results of the integration with the known value and obtain a correlation value as displayed on Equations 4.2 and 4.3. It should be noted that in the same article, they generate an additional step, an algorithm called map matching. In this case, they use the correction method using probabilities and calibration performed previously. To determine a range in which the particle, in this case, the individual, can be located after a certain number of steps. They then verify this against a map of the site, in their case, a shopping mall, to reduce the range and generate a higher probability of locating the person. For the purpose of this thesis, this last step was omitted, but it may be a method to consider for location on different maps modelled by the playing fields that would help generate a more accurate speed and distance value.

$$\mathbf{D} = 2\sqrt{2lh - h^2} \tag{4.1}$$

where l represents the length of the leg and h is the height of the subject.

$$\mathbf{D} = K \cdot \iint \mathbf{a}(t)dtdt \tag{4.2}$$

$$K = -\frac{D_g}{D_d} \tag{4.3}$$

where K represent the scaling factor D_g represents the proposed calibration distance, in this case 20m and D_d represents the distance obtained by integrating the signal.

The second algorithm does not take into account the magnitude of the acceleration but continues to treat them individually for each of the axes. It starts by processing the acceleration information in its vertical components and applies a transformation called Continuous Wavelet Transformation (CWT). This transformation allows an analysis of the signal in both the time and frequency components, which gives us information on the gait cycle. From the first transformation, step detection is possible. Similar to the previous method, a combination of local maxima detection is performed, which allows the extraction of the foot contact with the ground (IC). This is the main difference between both methods since it not only provides step detection but also the exact moment of foot contact with the ground. Another advantage of this method is that from a second transformation and detection of local maxima, it is possible to obtain the toe-off moment (TO). The extraction of these two features allows not only step detection but also to obtain other gait parameters, such as the identification of stance and swing time. Obtaining these moments allows us to combine and use other methods, such as zero-update hold from a sensor placed on the trunk. Therefore, it is possible to integrate the AP acceleration between the TO moment and the IC contact moment. That is to say, in the swing period, this allows for the correction of drift during the moment of foot stay and re-integrating from zero at the next detected step. In Figure 4.8 can be observed the signals generated by the transformations and the detection of the IC and TO moment to make the respective calculation of speed and distance travelled in each step. It is

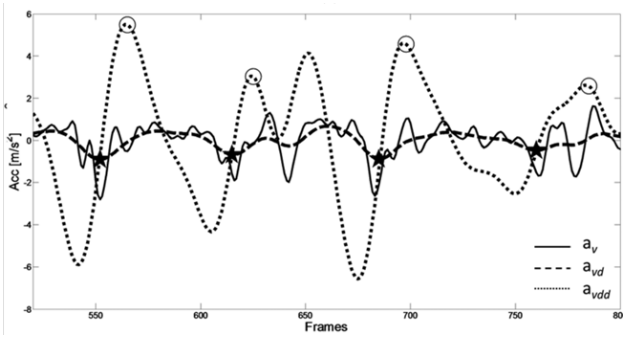


Figure 4.8: CWT Application on the Vertical Accelerometer Signal Walk, with a_V as the vertical acceleration, a_{vd} as the first CWT transformation, and a_{vdd} as the second CWT transformation with IC detected with circles as the IC and stars as the TO (Del Din et al., 2016)

worth mentioning that Pham et al. (2017) shows lower recognition results of the TO in the second transformation when the subject performed changes of direction on free-walk. However, this study

was performed with Parkinson's patients at speeds lower than the one aimed at this project. In the results chapter, we will make reference to the dataset for the TO recognition.

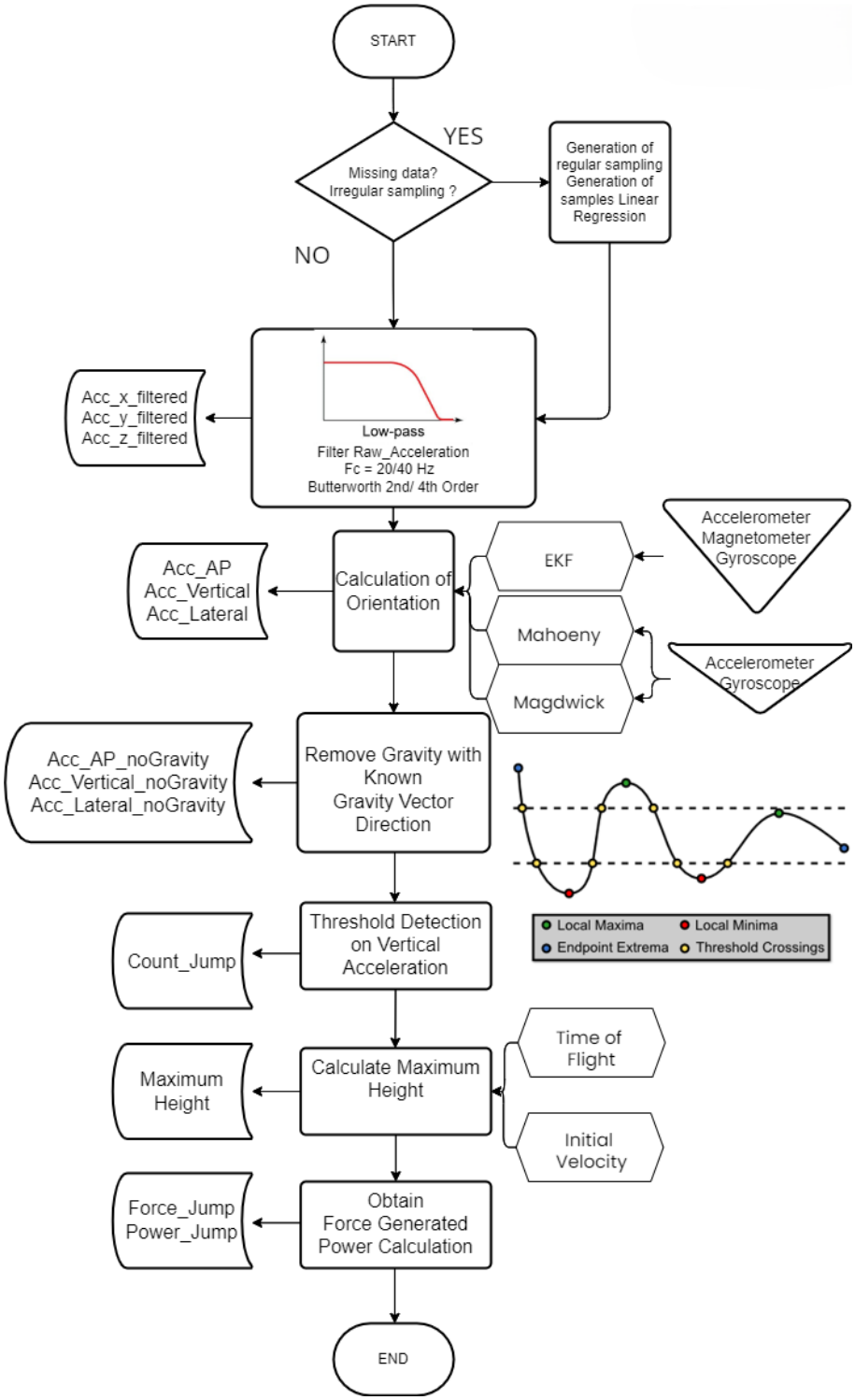


Figure 4.9: Workflow for Vertical Jump Metrics

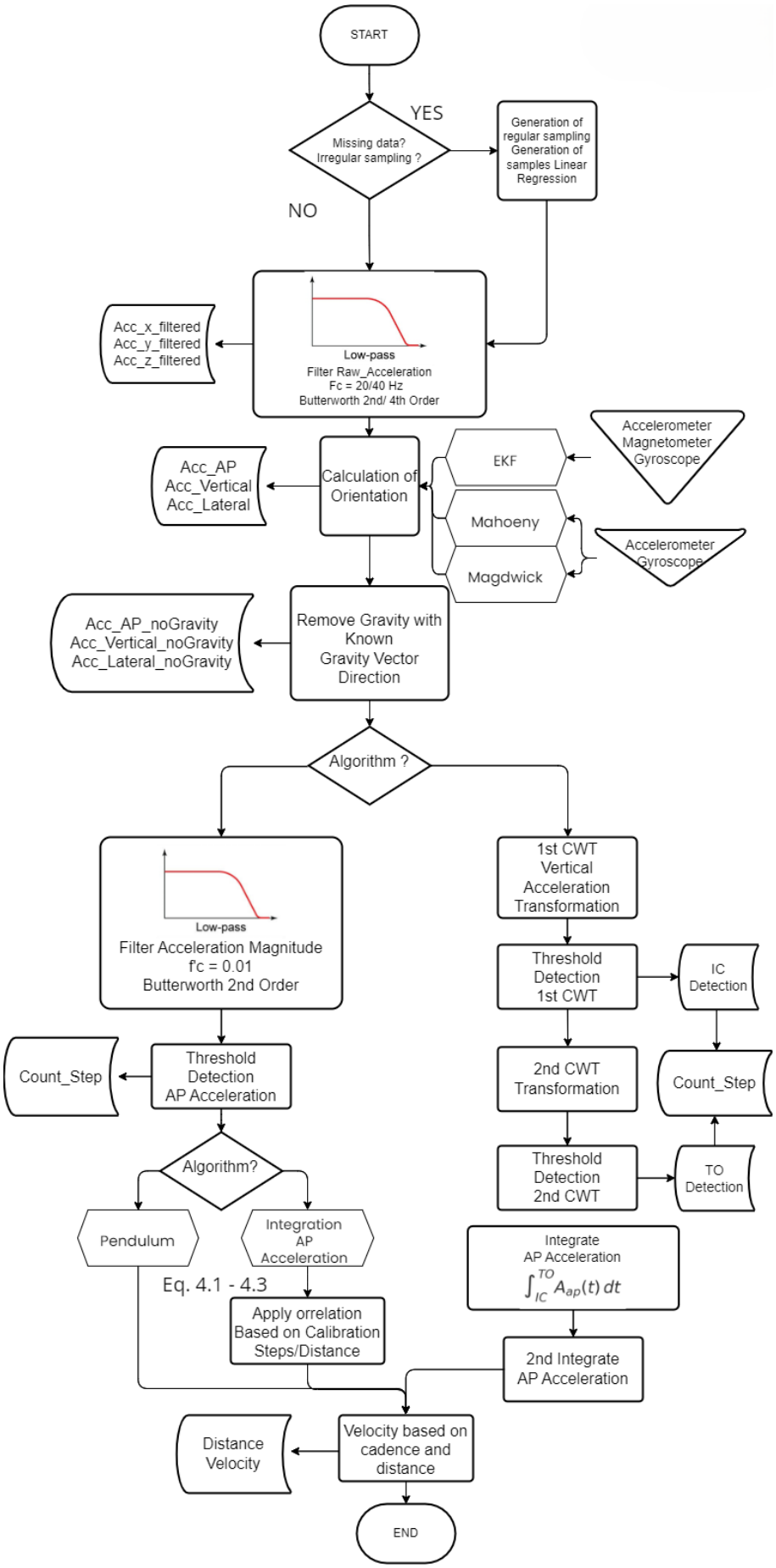


Figure 4.10: Workflow for Walk, Run Metrics

Chapter 5

Results and Discussion

5.1 Vertical Jump

This section shows the results obtained for the Vertical jump part. The validation was performed with only one measurement, maximum height. Since our device only has an accelerometer and gyroscope, we will limit ourselves in showing the data coming from these sensors for both datasets. Figures 5.1 and 5.3 show the processing performed focusing on the vertical acceleration for the Maule and Custom datasets, respectively. The first difference is that the Maule database presents the gravity acceleration in the negative Z axis, while the Custom dataset is in the direction of the negative Y axis. As mentioned in the methodology chapter, the corresponding transformation was applied to each dataset.

Based on movement on Figures 5.1 and 5.3 represent a stationary moment, the jump, and then still again. Therefore, the acceleration on the vertical axis at the beginning and at the end should be as close to zero as possible. Figures 5.1c and 5.3c show the same behaviour without any drift despite being a data acquisition of at least 15 seconds. Figures 5.1d and 5.3d show the detection of key points of the CMJ. The main peaks are those detected for the start and landing of the jump (red and green). These are only presented at the time of the jump in a given time interval, with a threshold value for the positive and negative part (we can see a trend in both for the case of a value of $15 m/s^2$ in the positive and the negative below $-20 m/s^2$).

The moment of the negative impulse of the jump was determined based on the detection of the maximum starting point of the jump, finding the minimum value prior to the maximum peak. The use of different thresholds was derived from the methodology based on Monnet et al. (2014). The threshold half-weight refers to the acceleration corresponding to half the weight removing the mass ($4.5 m/s^2$ in terms of vertical acceleration). This time was found by performing a linear regression with the values detected between the negative impulse peak and the maximum take-off peak. Thus, we are obtaining the take-off moment for this threshold. The same procedure was used for the landing point by changing the values by the negative of the value between the maximum take-off peak and the minimum of the landing peak. In the case of the zero-cross threshold, the only modification that the threshold was the first or the last zero-cross between the defined

parameters. This last approach is highly used for the force plates in the generation of maximum jump height.

For results obtained from the initial velocity method, we mainly use the impulse detection point shown in the figures 5.1d and 5.3d in conjunction with the zero-cross point described for the time methodology. The negative impulse methodology has a shorter integration time based on the fact that at the maximum bending moment, the subject lowers its centre of gravity and has a vertical velocity of zero. We are implementing the integration between this moment and the take-off. In the case of full-cycle integration, it detects the start of the jump impulse. It does this by generating two additional steps. Locating the maximum value before bending and then finding the first value that is above a threshold of the acceleration magnitude. That is to say, detecting the moment of the beginning of the jump movements. This is based on the fact that at the moment before the jump movement, the initial vertical velocity is zero. This assumption is of great help for drift correction in the case of the integration performed.

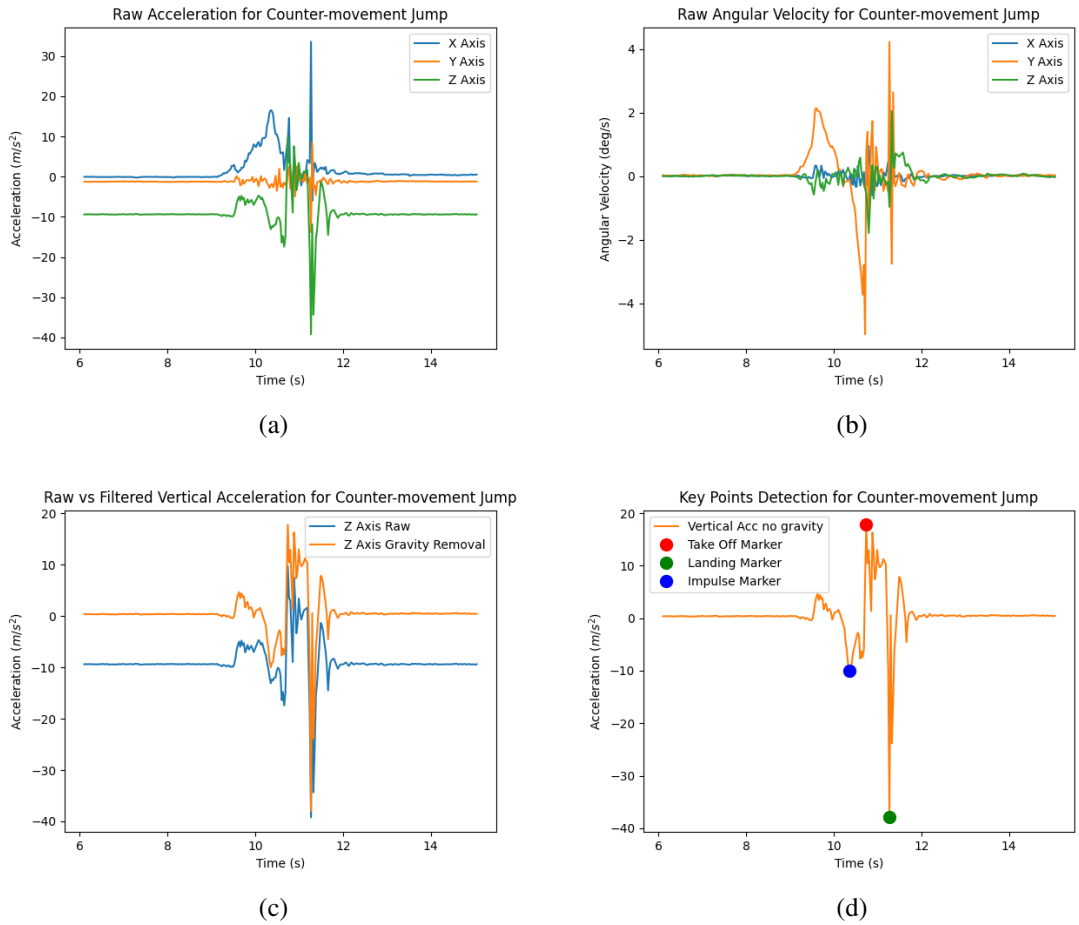


Figure 5.1: Data Representation for CMJ and Workflow on Maule Dataset a) Raw Accelerometer Data for a CMJ, b) Raw Gyroscope Data for a CMJ, c) Vertical Acceleration Data for a CMJ to visualize gravity removal, and d) Vertical Acceleration Data for a CMJ with Peak Detection to recognize the take-off, landing and impulse stages

The results obtained for both methods and datasets are in tables 5.1 and 5.2, represented with Bland Altman diagrams in Figures 5.2 and 5.4. Table 5.1 presents the data for the maximum height attained in the Maule dataset. It presents the ten jumps and their calculation with each of the methods. According to the comparison value, in this case, obtained by an optical instrument, the values of these jumps varied between 0.34 to 0.42m. With a mean of 0.39m.

In the case of the Maule Dataset, the time method with threshold zero-cross is the one that presents a lower error, only 6cm, and a low standard deviation compared to the rest of the algorithms. As shown in Figure 5.2b, there is no pattern in the data dispersion that indicates any alteration with jumps with greater or lesser height. Also, in Figure 5.2b, we can see that all the data are below 0 difference, indicating that the calculated values were always below the value of the optical instrument (gold standard). This could be due to a systematic bias, but with calibration/correction, the problem could be reduced. The same is true for the full impulse initial velocity method and the half-weight threshold time method (Figures 5.2a and 5.2d. The case that best evidences the systematic error is the initial velocity method with full impulse in Figure 5.2d. It presents a reduced interval of 95% reliability of 8cm with a difference of -29cm with respect to the value to be compared, meaning is precise but not accurate. In addition to the calibration necessary for the correction of the measurement, during the experiments carried out, it was noticed that although the database is described with an accelerometer reading of 75 Hz. At the moment of the start of the jump, the sampling becomes too unstable, obtaining sampling values close to 30-35 Hz. This generates that the values between the moments of integration, which in this case would be from the beginning of the movement to the take-off of the jump, are compromised, affecting the velocity and height values. Higher acceleration values should be obtained to correspond with the velocity, but the reduced sampling does not guarantee the correct acquisition of data in the moments of faster movements. This last factor significantly affects the initial velocity method with the negative impulse. It is during this moment that the jumping movement generates the greatest power, i.e., its fastest movement, which is when the subject reaches the point of maximum flexion, where the subject generates enough force to get up from the ground. This is also evidenced by figure 5.2c where the spread of the data for the impulse method seems to have a positive trend, i.e. for lower jump values, there is a higher reliability in the measurement, and as the jumps reach higher height values, the reliability of the algorithm decreases. Based on the proportional relationship that faster movements generate a greater height, the combination of jumps above 40cm combined with a sampling frequency below 40Hz does not guarantee a correct description of the movement for the implementation of the algorithm. Although the values were re-sampled with a constant frequency, using linear regression to complete the series does not prevent the loss of data.

The cause of irregular sampling can be several factors. Among them is the communication between the sensors or the microprocessor and the computer/server where the data processing is performed. For both datasets, the instruments work with the same technologies and communication protocol: a microprocessor in charge of the collection and communication between the sensors with an integrated Bluetooth module in charge of the transmission of data in real-time. Therefore, it is necessary to validate the size of the data to be sent, the sending rates, and the pro-

tocols that are capable of transmitting this information in the indicated periods of time. Another factor is the stability of the clock frequency of the oscillators in the microcontrollers. The quality of the oscillators determines the accuracy of the execution of instructions and the acquisition of data. Although these are not within the scope of study of the dissertation, due to prototype construction within the TexP@ct project, these were recommended and taken into account by the team in charge of the hardware construction.

	Time of Flight		**Initial Velocity**		
Jump	**1/2 Weight**	**Zero-Cross**	**Negative Impulse**	**Start Sequence**	**Optic**
Jump 1	0.27203253	0.321705182	0.078147838	0.128249487	0.39
Jump 2	0.34185888	0.345521929	0.034392206	0.142981565	0.39
Jump 3	0.34185888	0.326129095	0.338574025	0.107061611	0.40364
Jump 4	0.27434769	0.294892748	0.123606077	0.073240579	0.34669
Jump 5	0.21220992	0.367058204	0.290922424	0.103978647	0.4138
Jump 6	0.34315503	0.271073853	0.097852613	0.070255341	0.39309
Jump 7	0.3041149	0.344607777	0.091128831	0.109769241	0.414306
Jump 8	0.18555738	0.266493943	0.061187455	0.034174105	0.33962
Jump 9	0.38044284	0.376859572	0.442235049	0.13780006	0.420876
Jump 10	0.18460458	0.373267906	0.743545393	0.134493218	0.418876

Table 5.1: Results for Maximum Height Vertical Jump for Dataset Maule

	Time of Flight		**Initial Velocity**		
Jump	**1/2 Weight**	**Zero-Cross**	**Negative Impulse**	**Start Sequence**	**Xsens**
Jump 1	0.36556475	0.349577275	0.072028678	0.331251872	0.4127
Jump 2	0.36155859	0.35813167	0.061890821	0.360684561	0.4319
Jump 3	0.33669882	0.349565459	0.052597926	0.351203961	0.4114
Jump 4	0.3575745	0.365978929	0.062792596	0.344768186	0.4335
Jump 5	0.37499829	0.390880201	0.07487474	0.3729809	0.4572
Jump 6	0.29442263	0.409183081	0.092936354	0.363576984	0.4498
Jump 7	0.34967255	0.363405661	0.056094075	0.325198646	0.3261
Jump 8	0.39840863	0.424855474	0.173263625	0.358439892	0.3586
Jump 9	0.37364328	0.393530856	0.106632079	0.356814796	0.3428
Jump 10	0.264218525	0.37364328	0.077863026	0.341651986	0.4271

Table 5.2: Results for Maximum Height Vertical Jump for Dataset Personalized

The table 5.2 presents the results obtained for the customized dataset. The same methods were used as for the Maule dataset, changing the data acquisition instruments. In this case, the comparison value was obtained by the Xsens software, whose maximum height was between the range of 0.32m to 0.45m, with a mean of 0.41m. The results show the results for a subject performing 10 CMJ jumps.

The results of the figure 5.4, show again that the best method with the lowest error based on the measurement provided by Xsens is the time method with threshold zero-cross, since it presents an error of only 3 cm in a 5 cm interval of 95% reliability. The second best-performing algorithm was

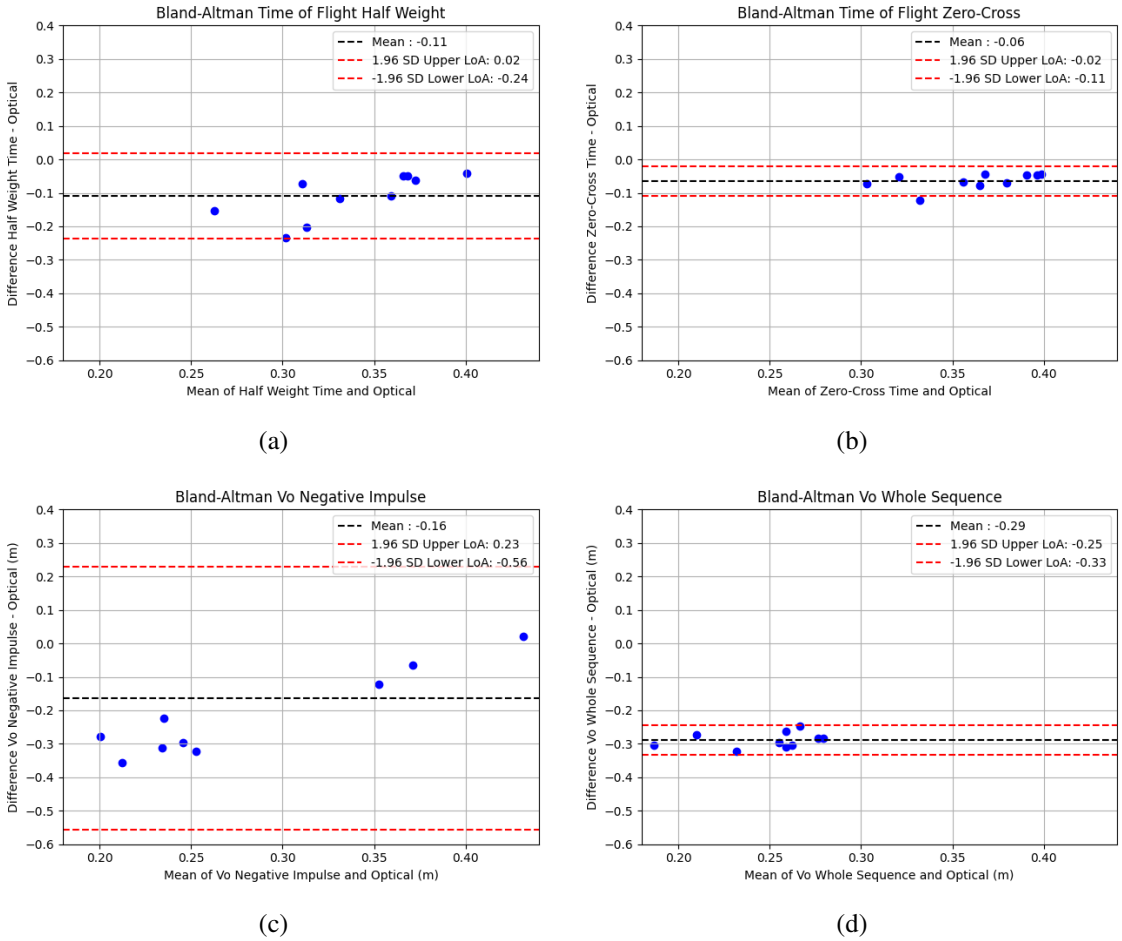


Figure 5.2: Bland-Altman Charts for Maule Dataset a) Bland-Altman Plot for Time of Flight with Threshold of Half-Weight vs Optical, b) Bland-Altman Plot for Time of Flight with threshold Zero-Cross vs Optical, c) Bland-Altman Plot for Vo Method with Negative Impulse vs Optical, and d) Bland-Altman Plot for Vo Method with Whole Impulse vs Optical

the full sequence integration of the jump in Figure (ref d). With a difference of 5cm and a range of 11 cm of 95% confidence. Unlike Figures 5.2b and 5.2d for the Maule set, Figures 5.4b and 5.4d do not present all of their data with a difference below zero. This means that there is no systematic error and that a calibration may not help to reduce the error. Another factor for Figures 5.4b and 5.4d is the dispersion of the data when the height estimation reaches a higher value, since these are always below the mean, unlike the jumps with a lower height. On the contrary, those with lower height are always above the difference of zero, indicating an overestimation. This variation in the difference can be corrected by adding a second evaluation layer. That is, the implementation of variable thresholds depends on the accelerations attained during the movement.

In spite of the customized database presenting an irregular sampling, being at a frequency of 1000Hz, a better reading of the accelerations in the moments of the jump was obtained. However, contrary results were presented in the initial velocity methods obtained. In the case of the complete sequence method, as shown in figure 5.4d, the error is limited to a difference of 5cm compared

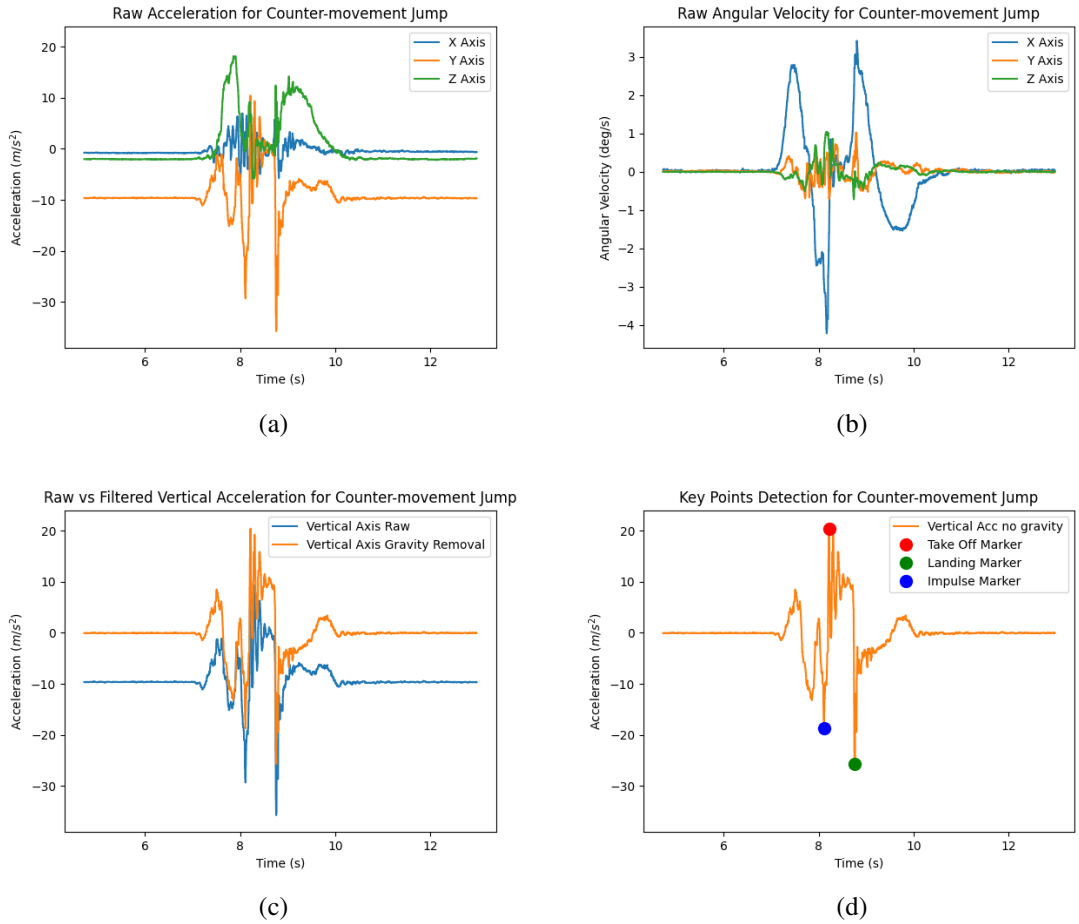


Figure 5.3: Data Representation for CMJ and Workflow on Personalized Dataset a) Raw Accelerometer Data for a CMJ, b) Raw Gyroscope Data for a CMJ, c) Vertical Acceleration Data for a CMJ to visualize gravity removal, and d) Vertical Acceleration Data for a CMJ with Peak Detection to recognize the take-off, landing and impulse stages

to the value of 29cm in Figure 5.2d. The opposite is the case for the negative impulse method, where the error went from 16 cm to 32 cm in Figures 5.2c and 5.4c, respectively. This could indicate that the detection of the impulse moments is not being performed properly, despite what is mentioned by the jumping platform methodologies described by Miranda-Oliveira et al. (2022). However, other variables, such as variability, have to be taken into account. In order to make such conclusions, more data is needed to validate whether this is an issue with the algorithm or simply an error in the data acquisition.

As mentioned in the methodology chapter, the implementation of both methods was due to the possible overestimation of the jump in case the final position was not the same as when the jump was initiated. However, for both datasets, with the time flight algorithms represented in the figures (5.2a, 5.2b and 5.4a, 5.4b) there is no tendency to overestimate the height of the jumps. In our case, it presents estimates below the value. In addition to the recommended calibration for the systematic error, other factors to consider are the modification of thresholds used within the

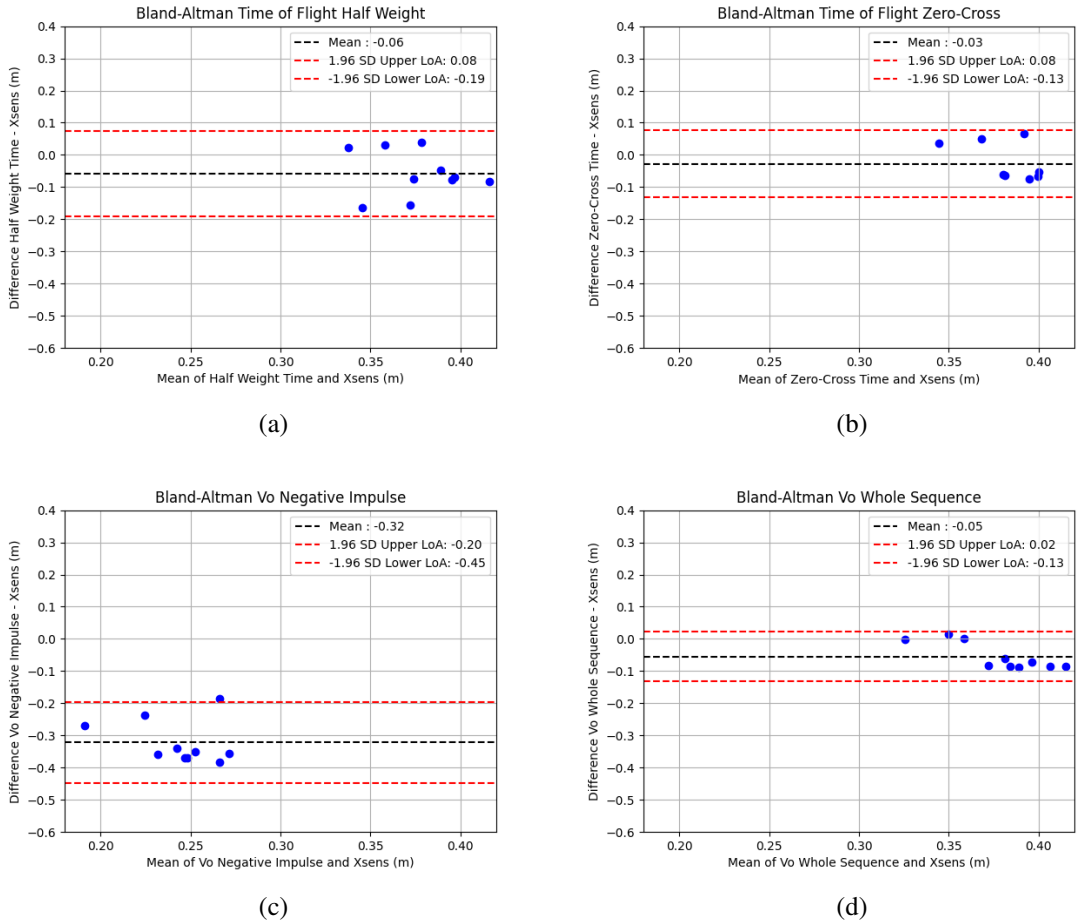


Figure 5.4: Bland-Altman Charts for Dataset Personalized a) Bland-Altman Plot for Time of Flight with Threshold of Half-Weight vs Xsens, b) Bland-Altman Plot for Time of Flight with threshold Zero-Cross vs Xsens, c) Bland-Altman Plot for Vo Method with Negative Impulse vs Xsens, and d) Bland-Altman Plot for Vo Method with Whole Impulse vs Xsens

algorithm, since these could increase the time of flight, reducing the sub-estimation error in the calculation of the maximum height obtained.

5.2 Walk and Run

The comparison value in this section will be the average speed attained during data acquisition. All datasets present data acquisition on treadmills to try to ensure a constant velocity for as long as possible. It is also worth mentioning that the average value was calculated, and only 50% of the detected movement time was taken into account. In other words, the first and last 25% of the data were discarded to avoid the transition values in the calculation of the final velocity. As in the case of the data sets used in the vertical jump section, two different databases were used, which presented different initial orientations of the gravity vector. However, this part of the algorithm is

not represented by any figure in this section since the results are the same as those presented in the vertical jump section.

Figures 5.5, 5.6, 5.7 and 5.8 represent the transformations needed for the CWT algorithm. Figure 5.5 presents the vertical acceleration along with the first Gaussian CWT with the 5th and 10th coefficients. These were selected based on the scale of values generated in the transform and the frequency selection described by Ji et al. (2019). The coefficients present the transform in time and frequency without any further modification. It was decided to use the 10th coefficient for the simplification of maximum point recognition. Both signals green and orange in Figure 5.5 are in synchronization with the vertical acceleration signal, which allows the recognition of contact points/step recognition. Both the first CWT signal and the second CWT signal, after obtaining the coefficients, were scaled for limiting values to facilitate the extraction of maxima for a range of databases with different velocities.

In Figure 5.6, we can see this scaling of the values for both transforms, together with the peak detection trend and the integrated velocity calculation. This image allows us to detect the phases of the stance and swing gait cycle. In this case, the blue signal peaks allow the recognition of the initial contacts, and the orange signal peaks the TO points. Figure 5.6 has the speed signal in green to identify when the signal value is being updated, important to have an interval between which could be obtained the value in real time. In the case of figure 5.7, which shows the same transformations as figure 5.6, only for the case of a higher speed, already considered as a run. Here the step frequency is higher, so increase the run update frequency and also its final value since it is close to 2.5 m/s or 9 km/h. The values of the 1st and 2nd CWT signals do not change due to the scaling of values mentioned above.

Both Figures 5.6 and 5.7 show times where the gait cycle detection is performed correctly but are cases where there is some step omission or erroneous detection. The algorithm used a time validation between consecutive steps and the nearest previous value. That is to say, at the moment of detecting an IC, it has to be accompanied by a TO value previously. This validation helped to reduce errors in recognition of gait stages, especially at the moment of the movement transitions (change in speed), as shown in Figure 5.8 between times 70 and 72 seconds on the 1st CWT. This transition generates the detection of an additional local maximum, which could generate an increase in the calculation of the estimated velocity.

For the step detection algorithm generated by the filtered acceleration magnitude, the results can be seen in Figures 5.9 and 5.10. Figure 5.9 presents the step detection in the case of a walking run at 4 km/h. The acceleration magnitude is represented in blue colour; this signal is then processed by the low-pass filter with a normalized frequency of 0.1 (orange colour), and then a peak detection corresponding (red colour) to the step detection is performed. 5.10 makes the same representation for the case of a signal with a speed at 9 km/h, which is why higher step peaks were detected in the same time interval as in Figure 5.9. In the case of the vertical scale we can find differences both in the magnitude of the acceleration and in the filtered signal. Since no scaling is performed in this algorithm, as opposed to the CWT method, during the evaluated intervals, no trend of erroneous step recognition at the moments of velocity change was identified. This does

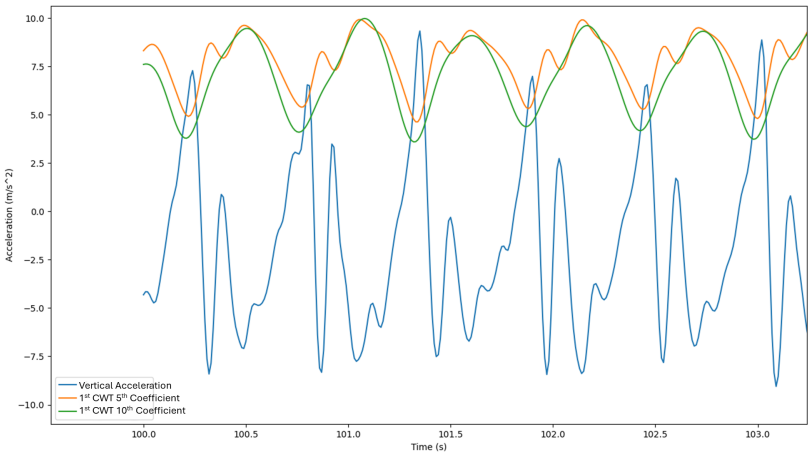


Figure 5.5: Continuous Wavelet Transform with different coefficients for IC Detection for Walking

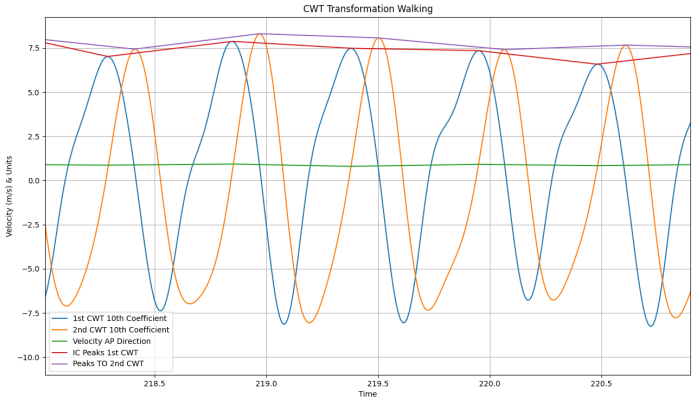


Figure 5.6: 1st and 2nd CWT for Gait Stages Detection in walk

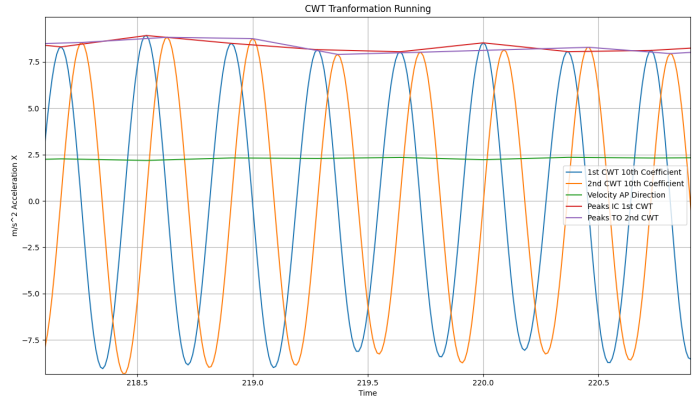


Figure 5.7: 1st and 2nd CWT for Gait Stages Detection in Run

not mean that the step recognition was more accurate, but that the filter response did not have as much variability compared to the speed range evaluated between 3 to 9 km/h.

For the results of the validation of the average velocity data obtained, it was decided to present the data through Bland-Altman diagrams in the figures 5.11 and 5.12. In this section, it was decided to use 4 different instances (2 for the CWT method and 2 for the filtered magnitude method). For the CWT method, the instances were based on different integration intervals. These were from each step (CWT one step) and from a double step (CWT Two Step). In the algorithm generated from the filtered magnitude signal, the two variants were in the step length estimation. One follows the CWT-like method using a sequential integration (Step Detection Magnitude), and the second from the pendulum method (Step Detection Ziljstra). In the case of both algorithms, a calibration factor was used in the calculation of the distance per step; in the case of the sequential integration, the same values mentioned in the article (Lu et al. (2019)) were used. In the case of the Ziljstra algorithm, the individual data were used in combination with the calibration of the mean estimation step. This is to have a representation of the entire population and not have to perform a calibration per subject, which would affect the results.

For the Korea dataset, the results are presented in Figure 5.11. The diagram presents the average speed results of each algorithm compared to the value provided by the treadmill for the 8 data captures. The method that presents the lowest error compared to the data provided by the treadmill was the CWT Two Step method represented in Figure 5.11b. This also presents the lowest range of data dispersion compared to the rest of the algorithms. The algorithm presented errors below 0.05m/s for the acquisitions that did not present any inclination, and all these estimations below the difference of 0m/s, that is to say, limited to the flat values, we can indicate a slight systematic value that can be corrected through a calibration. In this method no adjustment parameter was integrated, however, it could be added in the integration, similar to the one presented in equation 4.2. The algorithm represented by Figure 5.11a would be the method that would benefit the most from this adjustment because of how far away the mean difference value is. The algorithm with the second smallest error in the estimation of the final velocity was the Ziljstra algorithm. This is represented in Figure 5.11d and presents a fairly equal dispersion of data, which indicates that it may not be the most accurate algorithm, but it is very versatile when detecting these velocity changes.

The Hasso dataset presented the most data compared to the rest, presenting 27 data for each of the methods implemented for this metric. The Bland-Altman diagram is shown in the figure 5.12. The estimation method with the lowest error was the step detection method with accelerometer magnitude in combination with Zijstra step estimation represented in figure 5.12d with a mean difference of 0.01m/s. For the case of the methods represented in Figures 5.12a, 5.12c and 5.12d a trend can be identified regarding the spread of the data. There is an overestimation for low-velocity values and an underestimation for high-velocity values. This, in the same way that was discussed for the vertical jump height, could be reduced with the implementation of thresholds or variable calibrations. In the case of the Hasso dataset, the speed range indicated by the treadmill was between (2.8 to 5.7 km/h). In the case of the cwt two methods represented in figure 5.12c, it

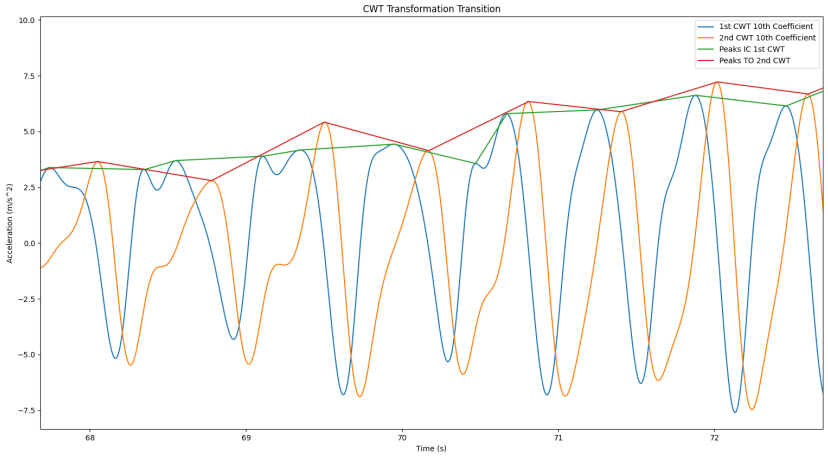


Figure 5.8: CWT Gait Stages Detection in Transition

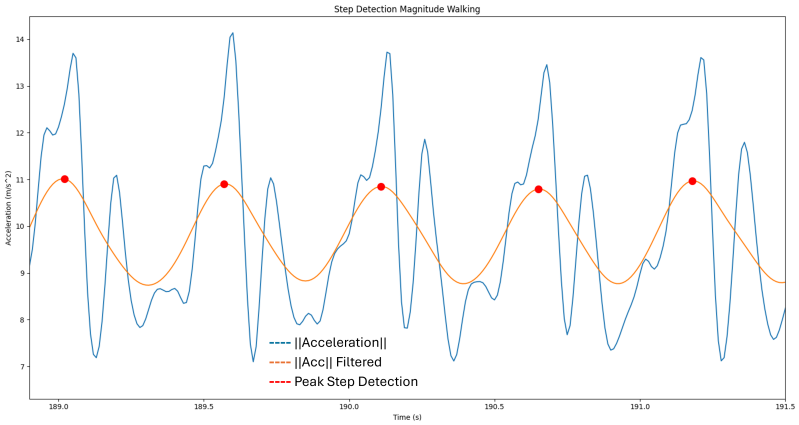


Figure 5.9: Step Detection with Filtered Magnitude Acceleration in Walk

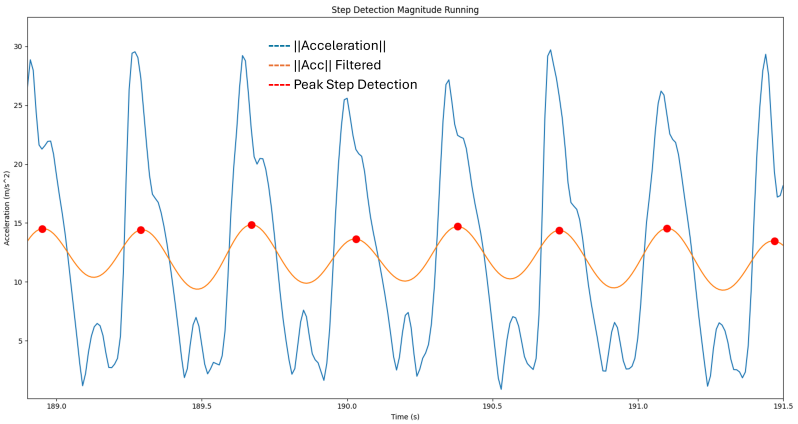


Figure 5.10: Step Detection with Filtered Magnitude Acceleration in Run

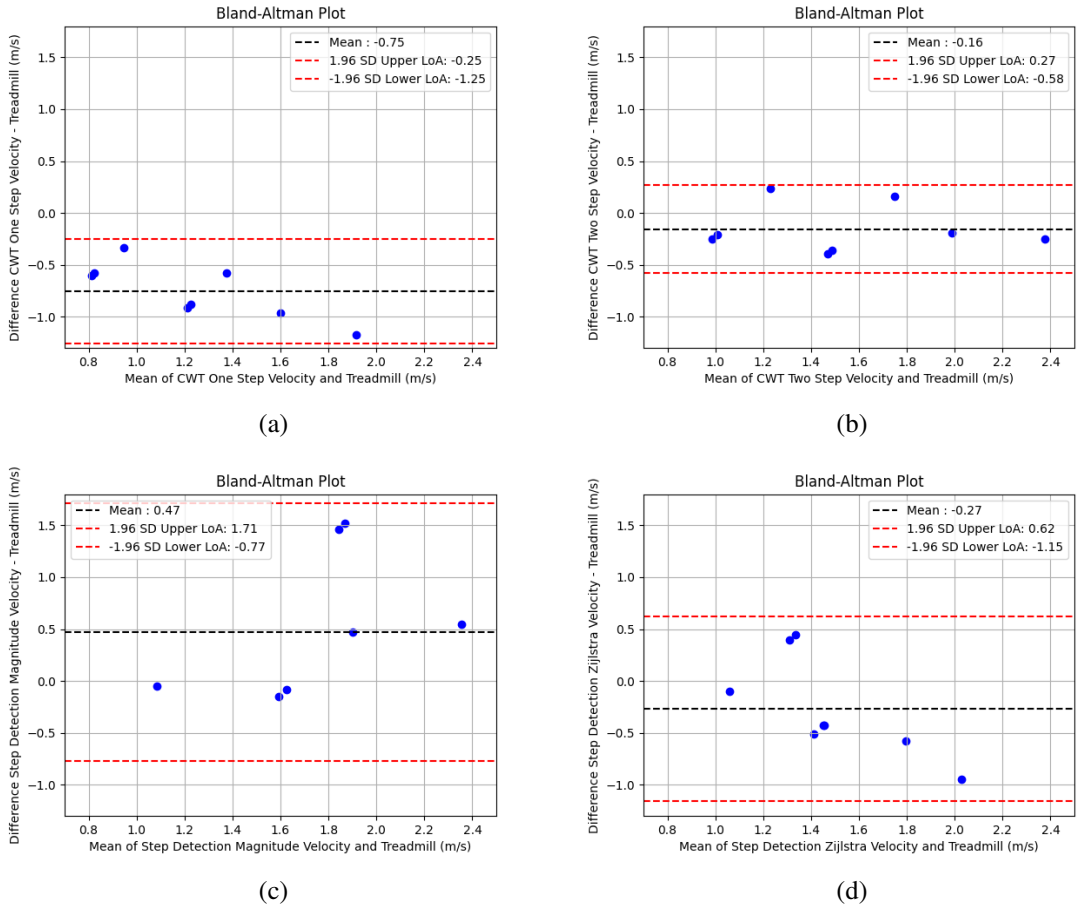


Figure 5.11: Bland-Altman Charts for Dataset Korea a) Bland-Altman Plot for CWT One Step vs Treadmill, b) Bland-Altman Plot for CWT Two Step vs Treadmill, c) Bland-Altman Plot for Step Detection by Magnitude vs Treadmill, and d) Bland-Altman Plot for Step Detection by Magnitude with Dijstra vs Treadmill

presents a phenomenon called heteroscedasticity. This means that it does not present a uniform variability among the data but a cone-shaped variability. In this case, a good accuracy for low velocity data and a lot of dispersion for high velocities. This brings a component of complexity since the implementation of threshold variables may not be a concrete solution because we cannot assume linear relationships, making the selection of parameters difficult. For this case we would have to perform an exploration using the Breusch–Pagan test to validate the heteroscedasticity and try to separate the data by groups to obtain a better estimation of the velocity value.

For the Hasso dataset, there were two circumstances that could have affected the velocity calculation. The first is that only one of the samples provided by IMU contained information of a previous static position, the rest of the data captures started already when the subject was moving. This is because the objective of the database was the correct detection of the gait instances and not the calculation of the velocity in our case. So, to try to reduce the drift in the AP acceleration component when the orientation calculation was performed, the initial orientation from the static

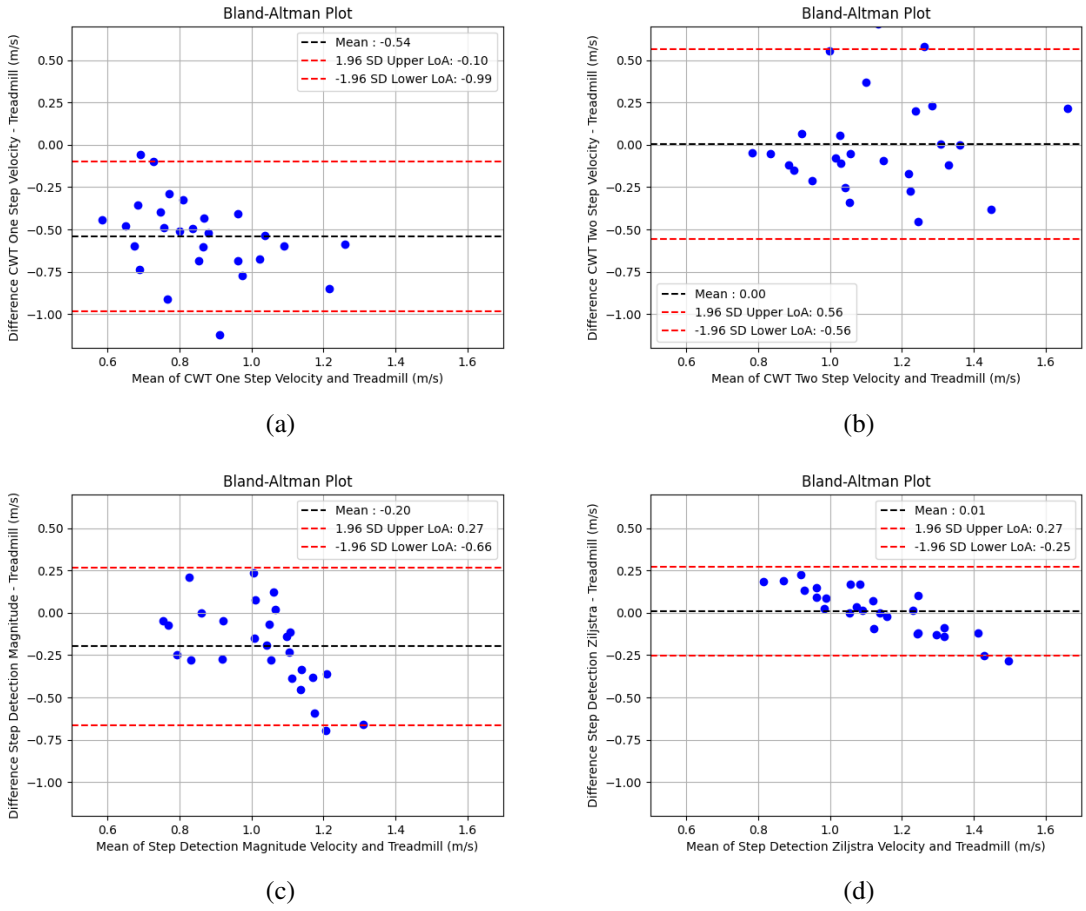


Figure 5.12: Bland-Altman Charts for Dataset Hasso a) Bland-Altman Plot for CWT One Step vs Treadmill, b) Bland-Altman Plot for CWT Two Step vs Treadmill, c) Bland-Altman Plot for Step Detection by Magnitude vs Treadmill, and d) Bland-Altman Plot for Step Detection by Magnitude with Dijstra vs Treadmill

subject was used as a reference for all other captures. The second factor that could be a possible explanation for the poor performance of the CWT algorithm in this database is due to the incorrect moment localization of T0 detected with the second transformation. Based on what was reported by Del Din et al. (2016) and Pham et al. (2017), this is based on the fact that the algorithm presented a greater measure of error when the subject walked at plus-minus 20% of the preferential velocity value. This is based on the study Beauchet et al. (2009) where a step asymmetry rises with speed variations. This is based on Table 5.3 where the mean difference of each of the acquisitions is indicated, and in the case of the preferential speed, the mean error is -0.02 m/s.

	PWS–20% (m/s)	**PWS (m/s)**	**PWS+20% (m/s)**
Mean (Two Step CWT-Treadmill)	0.120050718	-0.021728672	-0.089881162

Table 5.3: Mean Velocity Difference between Two Step CWT - Treadmill

The last test performed was the combination of both methods to recognize both movements in the same sequence. This was successful, as shown in Figure 5.13. This only shows the detection of the jump, however a more detailed experimentation will be carried out for validation, specially with the initial velocity whole sequence method. This sequence was captured with the settings of the personalized dataset.

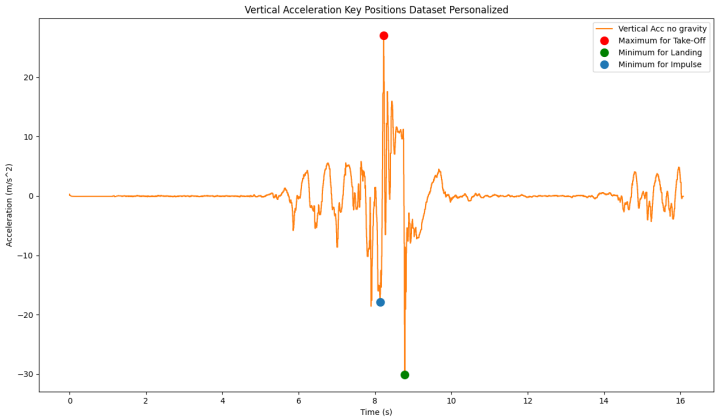


Figure 5.13: Walk and Jump Sequence with Jump Detection

Chapter 6

Conclusions and Next Steps

Based on the context in which the project is being developed and on the objectives proposed for this research work. We can indicate that these were achieved and that the results are promising since the metrics of maximum height and running speed will allow athletes/coaches to have quantitative indicators that describe physical activity. Movements such as walking, running and jumping are performed during physical education classes as well as training sports, thus allowing a range of different activities to be evaluated.

In the specific case of the jumping algorithms, we managed to validate the application of both algorithms (Time of flight and Initial velocity) in our own database, which will allow the subsequent adjustment and calibration for future tests and will undoubtedly improve the performance of the metrics obtained by these. It should be noted that among the variables to be considered it is very important that the data sampling is obtained as constant as possible and with a sampling rate equal to or greater than 200 Hz. This last factor is crucial, especially in the case of using initial velocity at the time of acceleration integration. In case we want to continue with the exploration of the initial velocity method from the negative impulse within the suggestions, we should evaluate the use of different values of thresholds similar to what was done in the study Monnet et al. (2014) with the flight times. This is with the objective of reducing the drift by a shorter integration time. Another recommendation for future testing is the evaluation of a wider range of thresholds for the time of flight. As indicated in the discussion, the systematic error presented during the zero-cross method could be corrected by the zero-cross method and achieve more accurate values of maximum height.

During the jump evaluation we were also able to obtain power and force values generated as indicated. Therefore, one of the steps would be the validation of these values through a force plate. That would allow us to compare the values obtained by our algorithm versus the force plate. With the objective of validating the proportional relation of variables and the selection of the best method for the final calculation of these. Within the tests to be integrated, we will also have to evaluate other types of jumps, such as horizontal and vertical speed jumps, and evaluate if the algorithms used can be extrapolated to these other types of jumps. The review of other alternative methods such as the implementation of artificial intelligence may be necessary for these jumps,

however, it would bring the condition of generation training data.

In the specific case of the walking and running algorithms. It was possible to correctly apply the step and distance detection algorithms performed for each of these to calculate average speed. The results highlighted the number of variables that affected the calculations such as initial calibration, the inclination at the time of the trajectory and speed variability. Therefore, one of the recommendations would be the evaluation of each of these variables separately in order to obtain better conclusions about the algorithms and their selection. It should be noted that in this study, the same drawbacks were not identified in the lack of constant sampling since both showed better results in relation to this aspect. However, maintaining a sampling rate of 200 Hz would be of great help to guarantee the quality of the velocity estimation. Since no experimentation of velocity has been done with the hardware developed by Plux, the next step would be the validation in a similar environment/settings to the datasets previously used.

Another factor to take into account is the implementation of the variable thresholds, especially for the extreme values, taking into account that within the project, there will be a previous classification based on artificial intelligence algorithms that recognize when static, running, or walking could be a probable filter for the implementation of these. This same classification can be used for the CWT method that presented heteroscedasticity since this grouping could allow the generation of different patterns or coefficients to be used and obtain more accurate measurements. Within the same CWT method, further experimentation is necessary for the correct detection of TO points. This would require a different methodology as it would involve a more robust analysis of the gait cycle, focusing on the detection of the stay and swing moments. A greater robustness in the correct detection of these points would generate a proportionate effect on the velocity calculation for both methods. Finally, within the CWT algorithm, both step distance calculation methods could be integrated, integrating the scaling factors. A statistical description for each of these runs and not an overview of the data might become necessary at the time of this experimentation.

One of the general conclusions for both metrics is the generation of more data to allow a considerable number to obtain more robust conclusions about the algorithms and metrics to be detected. Generating these data under the same conditions as the comparison methods. That is to say that the data sampling is the same, the IMU position is the same and the collection protocols are the same. Given the importance of generating data, we resorted in conjunction with the faculty of sport for the generation of a pilot methodology for future data collection. It is worth mentioning that it is still in draft version, however I attach a summary with some key factors.

The data collection for the prototype update will last 10 months. It is expected to start during the month of July. The methodology is based on 2 fully functional prototypes that allow the capture of data from one subject while the next one is performing the validation tests. The validation instruments will be the Xsense suit and the Polar H10 device. The experimentation will consist of several exercises of a battery of tests called FITESCOLA[1]. The experiments will be performed on 30 subjects, varying the sex and limiting to 10 people between the ranges of (12-14, 14-16, and 16-18) to have a representation of the entire target population of the final product. Within the data

[1] https://fitescola.dge.mec.pt/home.aspx

analysis, the application of statistics such as t-test, means of final values, percentages of error and standard deviation are highlighted. Bland-Altman graphs used in this dissertation and correlation diagrams between classes will also be included.

Within the context of the TexP@ct project, several additional evaluation metrics are included in addition to those obtained for the jump and run. Such as activity recognition and intensity levels. These were included in the literature review of the work initially, however, in conjunction with my advisor it was decided to focus on the metrics of characterization of jumping and running and other collaborators are making the additional metrics. One of the last steps before the end of the project will be the generation of a database file in Zenodo, which will allow not only for future iterations of the project. But to promote more research in this area by facilitating access to information and generating more knowledge about it.

In parallel to the data collection, a package of functions will be generated that will serve as an application programming interface (API) for the integration of the calculation algorithms with the application that is being developed by the HumanISE team of INESCTEC to show results and keep track of the records.

References

Jassim Almulla, Abdulrahman Takiddin, and Mowafa Househ. The use of technology in tracking soccer players' health performance: a scoping review. *BMC Medical Informatics and Decision Making*, 20:184, August 2020. ISSN 1472-6947. doi: 10.1186/s12911-020-01156-4. URL https://www.ncbi.nlm.nih.gov/pmc/articles/PMC7422501/.

Andy Ruina and Rudra Pratap. *Introduction to Statics and Dynamics*. Oxford University Press, 2010. URL http://archive.org/details/ost-engineering-ruinapratap8-21-10.

Md Arif Anwary, Hongnian Yu, and Michael Vassallo. An Automatic Gait Feature Extraction Method for Identifying Gait Asymmetry Using Wearable Sensors. *Sensors*, 18:676, February 2018. doi: 10.3390/s18020676.

Katya Arquilla, Andrea K. Webb, and Allison P. Anderson. Textile Electrocardiogram (ECG) Electrodes for Wearable Health Monitoring. *Sensors*, 20(4):1013, January 2020. ISSN 1424-8220. doi: 10.3390/s20041013. URL https://www.mdpi.com/1424-8220/20/4/1013. Number: 4 Publisher: Multidisciplinary Digital Publishing Institute.

G. P. Bailey and R. K. Harle. Sampling Rates and Sensor Requirements for Kinematic Assessment During Running Using Foot Mounted IMUs. In Jan Cabri, João Barreiros, and Pedro Pezarat Correia, editors, *Sports Science Research and Technology Support*, Communications in Computer and Information Science, pages 42–56, Cham, 2015. Springer International Publishing. ISBN 978-3-319-25249-0. doi: 10.1007/978-3-319-25249-0_4.

R. Baranek. Inertial Measurement Unit – Data Fusion and Visualization using MATLAB. *IFAC Proceedings Volumes*, 45(7):12–16, January 2012. ISSN 1474-6670. doi: 10.3182/20120523-3-CZ-3015.00005. URL https://www.sciencedirect.com/science/article/pii/S1474667015350540.

Olivier Beauchet, Cedric Annweiler, Yhann Lecordroch, Gilles Allali, Veronique Dubost, François R Herrmann, and Reto W Kressig. Walking speed-related changes in stride time variability: effects of decreased speed. *Journal of NeuroEngineering and Rehabilitation*, 6:32, August 2009. ISSN 1743-0003. doi: 10.1186/1743-0003-6-32. URL https://www.ncbi.nlm.nih.gov/pmc/articles/PMC2731039/.

Lauren C. Benson, Christian A. Clermont, Eva Bošnjak, and Reed Ferber. The use of wearable devices for walking and running gait analysis outside of the lab: A systematic review. *Gait & Posture*, 63:124–138, June 2018a. ISSN 0966-6362. doi: 10.1016/j.gaitpost.2018.04.047. URL https://www.sciencedirect.com/science/article/pii/S0966636218304715.

Lauren C. Benson, Christian A. Clermont, Sean T. Osis, Dylan Kobsar, and Reed Ferber. Classifying running speed conditions using a single wearable sensor: Optimal segmentation and feature extraction methods. *Journal of Biomechanics*, 71:94–99, April 2018b. ISSN 0021-9290. doi: 10.1016/j.jbiomech.2018.01.034. URL https://www.sciencedirect.com/science/article/pii/S0021929018300678.

Thiago O. Borges, Alexandre Moreira, Renato Bacchi, Ronaldo L. Finotti, Mayara Ramos, Charles R. Lopes, and Marcelo S. Aoki. Validation of the VERT wearable jump monitor device in elite youth volleyball players. *Biology of Sport*, 34(3):239–242, 2017. ISSN 0860-021X, 2083-1862. doi: 10.5114/biolsport.2017.66000. URL https://www.termedia.pl/Validation-of-the-VERT-wearable-jump-monitor-device-in-elite-youth-volleyball-players,78,29498,1,1.html. Publisher: Termedia.

Laura Bowen, Aleksander Stefan Gross, Mo Gimpel, and François-Xavier Li. Accumulated workloads and the acute:chronic workload ratio relate to injury risk in elite youth football players. *British Journal of Sports Medicine*, 51(5):452–459, March 2017. ISSN 0306-3674, 1473-0480. doi: 10.1136/bjsports-2015-095820. URL https://bjsm.bmj.com/content/51/5/452. Publisher: BMJ Publishing Group Ltd and British Association of Sport and Exercise Medicine Section: Original article.

Luke J. Boyd, Kevin Ball, and Robert J. Aughey. The reliability of MinimaxX accelerometers for measuring physical activity in Australian football. *International Journal of Sports Physiology and Performance*, 6(3):311–321, September 2011. ISSN 1555-0265. doi: 10.1123/ijspp.6.3.311.

Soren Brage, N Brage, P.W. Franks, Ulf Ekelund, and N.J. Wareham. Brage S, Brage N, Franks PW, Ekelund U, Wareham NJ. Reliability and validity of the combined heart rate and movement sensor Actiheart. Eur J Clin Nutr 59, 561-570. *European journal of clinical nutrition*, 59:561–70, April 2005. doi: 10.1038/sj.ejcn.1602118.

Thomas Brunner, Jean-Philippe Lauffenburger, Sébastien Changey, and Michel Basset. Magnetometer-Augmented IMU Simulator: In-Depth Elaboration. *Sensors*, 15(3):5293–5310, March 2015. ISSN 1424-8220. doi: 10.3390/s150305293. URL https://www.mdpi.com/1424-8220/15/3/5293. Number: 3 Publisher: Multidisciplinary Digital Publishing Institute.

Andreas Bulling, Ulf Blanke, and Bernt Schiele. A tutorial on human activity recognition using body-worn inertial sensors. *ACM Computing Surveys*, 46(3):1–33, January 2014. ISSN 0360-0300, 1557-7341. doi: 10.1145/2499621. URL https://dl.acm.org/doi/10.1145/2499621.

Damjana V. Cabarkapa, Dimitrije Cabarkapa, Drake A. Eserhaut, and Andrew C. Fry. Relationship between internal and external load metrics in professional male basketball players. *Journal of Human Sport and Exercise*, 18(4), 2023. ISSN 1988-5202. doi: 10.14198/jhse.2023.184.01. URL http://hdl.handle.net/10045/133938.

Carlo Castagna, Marco Ganzetti, Massimiliano Ditroilo, Marco Giovannelli, Alessandro Rocchetti, and Vincenzo Manzi. Concurrent Validity of Vertical Jump Performance Assessment Systems. *The Journal of Strength & Conditioning Research*, 27 (3):761, March 2013. ISSN 1064-8011. doi: 10.1519/JSC.0b013e31825dbcc5. URL

https://journals.lww.com/nsca-jscr/fulltext/2013/03000/concurrent_validity_of_vertical_jump_performance.28.aspx.

David Castells-Rufas and Jordi Carrabina. Simple real-time QRS detector with the MaMeMi filter. *Biomedical Signal Processing and Control*, 21:137–145, August 2015. ISSN 17468094. doi: 10.1016/j.bspc.2015.06.001. URL https://linkinghub.elsevier.com/retrieve/pii/S1746809415001032.

Wei-Han Chen, Chun-Wei Chiang, Nicholas J. Fiolo, Philip X. Fuchs, and Tzyy-Yuang Shiang. Ideal Combinations of Acceleration-Based Intensity Metrics and Sensor Positions to Monitor Exercise Intensity under Different Types of Sports. *Sensors*, 22(7):2583, January 2022. ISSN 1424-8220. doi: 10.3390/s22072583. URL https://www.mdpi.com/1424-8220/22/7/2583. Number: 7 Publisher: Multidisciplinary Digital Publishing Institute.

Christophe Coillot and Paul Leroy. Induction Magnetometers Principle, Modeling and Ways of Improvement. In *Magnetic Sensors - Principles and Applications*. IntechOpen, March 2012. ISBN 978-953-51-0232-8. doi: 10.5772/38945. URL https://www.intechopen.com/chapters/30943.

Heidi Compton, Jace Delaney, Grant Duthie, Andre Nelson, and Fabio Serpiello. Inter-Unit Reliability and Effect of Data Processing Methods of Global Positioning Systems. *International Journal of Sports Physiology and Performance*, 14, August 2018. doi: 10.1123/ijspp.2018-0273.

Zachary L. Crang, Grant Duthie, Michael H. Cole, Jonathon Weakley, Adam Hewitt, and Rich D. Johnston. The inter-device reliability of global navigation satellite systems during team sport movement across multiple days. *Journal of Science and Medicine in Sport*, 25(4):340–344, April 2022. ISSN 14402440. doi: 10.1016/j.jsams.2021.11.044. URL https://linkinghub.elsevier.com/retrieve/pii/S1440244021005338.

Scott E. Crouter, Kurt G. Clowers, and David R. Bassett. A novel method for using accelerometer data to predict energy expenditure. *Journal of Applied Physiology*, 100 (4):1324–1331, April 2006. ISSN 8750-7587. doi: 10.1152/japplphysiol.00818.2005. URL https://journals.physiology.org/doi/full/10.1152/japplphysiol.00818.2005. Publisher: American Physiological Society.

Cloe Cummins, Rhonda Orr, Helen O'Connor, and Cameron West. Global Positioning Systems (GPS) and Microtechnology Sensors in Team Sports: A Systematic Review. *Sports medicine (Auckland, N.Z.)*, 43, June 2013. doi: 10.1007/s40279-013-0069-2.

Terje Dalen, Ingebrigtsen Jørgen, Ettema Gertjan, Hjelde Geir Havard, and Wisløff Ulrik. Player Load, Acceleration, and Deceleration During Forty-Five Competitive Matches of Elite Soccer. *The Journal of Strength & Conditioning Research*, 30 (2):351, February 2016. ISSN 1064-8011. doi: 10.1519/JSC.0000000000001063. URL https://journals.lww.com/nsca-jscr/fulltext/2016/02000/player_load,_acceleration,_and_deceleration_during.8.aspx.

Majid Ddafshar. Accelerometer and Gyroscopes Sensors: Operation, Sensing, and Applications | Analog Devices, 2014. URL https://www.analog.com/en/technical-articles/accelerometer-and-gyroscopes-sensors-operation-sensing-and-applications.html.

Silvia Del Din, Alan Godfrey, and Lynn Rochester. Validation of an Accelerometer to Quantify a Comprehensive Battery of Gait Characteristics in Healthy Older Adults and Parkinson's Disease: Toward Clinical and at Home Use. *IEEE journal of biomedical and health informatics*, 20(3):838–847, May 2016. ISSN 2168-2208. doi: 10.1109/JBHI.2015.2419317.

Maxime Devanne, Panagiotis Papadakis, and Sao Mai Nguyen. *Recognition of Activities of Daily Living via Hierarchical Long-Short Term Memory Networks*. October 2019. doi: 10.1109/SMC.2019.8914457. Pages: 3324.

Robert DiPietro and Gregory D. Hager. Chapter 21 - Deep learning: RNNs and LSTM. In S. Kevin Zhou, Daniel Rueckert, and Gabor Fichtinger, editors, *Handbook of Medical Image Computing and Computer Assisted Intervention*, The Elsevier and MICCAI Society Book Series, pages 503–519. Academic Press, January 2020. ISBN 978-0-12-816176-0. doi: 10.1016/B978-0-12-816176-0.00026-0. URL https://www.sciencedirect.com/science/article/pii/B9780128161760000260.

Seth R. Donahue and Michael E. Hahn. Validation of Running Gait Event Detection Algorithms in a Semi-Uncontrolled Environment. *Sensors (Basel, Switzerland)*, 22(9):3452, April 2022. ISSN 1424-8220. doi: 10.3390/s22093452. URL https://www.ncbi.nlm.nih.gov/pmc/articles/PMC9101903/.

R. G. Eston, A. V. Rowlands, and D. K. Ingledew. Validity of heart rate, pedometry, and accelerometry for predicting the energy cost of children's activities. *Journal of Applied Physiology (Bethesda, Md.: 1985)*, 84(1):362–371, January 1998. ISSN 8750-7587. doi: 10.1152/jappl.1998.84.1.362.

Luis Fernández-Galván, Arturo Casado, Amador García Ramos, and Guy Haff. Effects of Vest and Sled Resisted Sprint Training on Sprint Performance in Young Soccer Players: A Systematic Review and Meta-analysis. *Journal of Strength and Conditioning Research*, Publish Ahead of Print, April 2022. doi: 10.1519/JSC.0000000000004255.

Alessandro Filippeschi, Norbert Schmitz, Markus Miezal, Gabriele Bleser, Emanuele Ruffaldi, and Didier Stricker. Survey of Motion Tracking Methods Based on Inertial Sensors: A Focus on Upper Limb Human Motion. *Sensors*, 17(6):1257, June 2017. ISSN 1424-8220. doi: 10.3390/s17061257. URL https://www.mdpi.com/1424-8220/17/6/1257. Number: 6 Publisher: Multidisciplinary Digital Publishing Institute.

Fitbit LLC. Check your heart rate | Fitbit Luxe User Manual, 2023. URL https://help.fitbit.com/manuals/luxe/Content/manuals/Topics/Exercise%20and%20Heart%20Health/Check%20your%20heart%20rate.htm.

Carol Ewing Garber, Bryan Blissmer, Michael R. Deschenes, Barry A. Franklin, Michael J. Lamonte, I.-Min Lee, David C. Nieman, and David P. Swain. Quantity and Quality of Exercise for Developing and Maintaining Cardiorespiratory, Musculoskeletal, and Neuromotor Fitness in Apparently Healthy Adults: Guidance for Prescribing Exercise. *Medicine & Science in Sports & Exercise*, 43(7):1334, July 2011. ISSN 0195-9131. doi: 10.1249/MSS.0b013e318213fefb. URL https://journals.lww.com/acsm-msse/fulltext/2011/07000/quantity_and_quality_of_exercise_for_developing.26.aspx.

Garmin Ltd. vívoactive 4/4S - Cálculos da zona de frequência cardíaca, 2019. URL https://www8.garmin.com/manuals/webhelp/vivoactive4_4S/PT-BR/GUID-A8716C0B-B267-4C42-B45F-B9C7928BCA19.html.

Jeremy A. Gentles, Christine L. Coniglio, Matthew M. Besemer, Joshua M. Morgan, and Michael T. Mahnken. The Demands of a Women's College Soccer Season. *Sports*, 6(1):16, March 2018. ISSN 2075-4663. doi: 10.3390/sports6010016. URL https://www.mdpi.com/2075-4663/6/1/16. Number: 1 Publisher: Multidisciplinary Digital Publishing Institute.

Marlène Giandolini, Sébastien Pavailler, Pierre Samozino, Jean-Benoît Morin, and Nicolas Horvais. Foot strike pattern and impact continuous measurements during a trail running race: proof of concept in a world-class athlete. *Footwear Science*, 7(2):127–137, May 2015. ISSN 1942-4280. doi: 10.1080/19424280.2015.1026944. URL https://doi.org/10.1080/19424280.2015.1026944. Publisher: Taylor & Francis _eprint: https://doi.org/10.1080/19424280.2015.1026944.

Periklis Gogas. *Machine Learning - Introduction to Classification*. September 2022. doi: 10.13140/RG.2.2.19990.63045.

Rui Jorge Pereira Gonçalves. Multivariate Time Series Analysis with Deep Learning. July 2021. URL https://repositorio-aberto.up.pt/handle/10216/135947. Accepted: 2022-09-10T10:07:01Z.

Cam Gordon. Quaternion Representation of 3D Orientation and Rotation for Sensor Fusion Applications. 2021.

Saurabh Gupta. Deep learning based human activity recognition (HAR) using wearable sensor data. *International Journal of Information Management Data Insights*, 1(2):100046, November 2021. ISSN 2667-0968. doi: 10.1016/j.jjimei.2021.100046. URL https://www.sciencedirect.com/science/article/pii/S2667096821000392.

Carlos D. Gómez-Carmona, José Pino-Ortega, Braulio Sánchez-Ureña, Sergio J. Ibáñez, and Daniel Rojas-Valverde. Accelerometry-Based External Load Indicators in Sport: Too Many Options, Same Practical Outcome? *International Journal of Environmental Research and Public Health*, 16(24):5101, January 2019. ISSN 1660-4601. doi: 10.3390/ijerph16245101. URL https://www.mdpi.com/1660-4601/16/24/5101. Number: 24 Publisher: Multidisciplinary Digital Publishing Institute.

Carlos D. Gómez-Carmona, Alejandro Bastida-Castillo, Sergio J. Ibáñez, and José Pino-Ortega. Accelerometry as a method for external workload monitoring in invasion team sports. A systematic review. *PLOS ONE*, 15(8):e0236643, August 2020. ISSN 1932-6203. doi: 10.1371/journal.pone.0236643. URL https://dx.plos.org/10.1371/journal.pone.0236643.

Vedran Hadžić, Aleš Germič, and Aleš Filipčič. Validity and reliability of a novel monitoring sensor for the quantification of the hitting load in tennis. *PLoS ONE*, 16(7):e0255339, July 2021. ISSN 1932-6203. doi: 10.1371/journal.pone.0255339. URL https://www.ncbi.nlm.nih.gov/pmc/articles/PMC8321100/.

Chaolei Han, Lei Zhang, Yin Tang, Wenbo Huang, Fuhong Min, and Jun He. Human activity recognition using wearable sensors by heterogeneous convolutional neural networks. *Expert Systems with Applications*, 198:116764, July 2022. ISSN 0957-4174. doi: 10.1016/j.eswa.2022.116764. URL https://www.sciencedirect.com/science/article/pii/S0957417422002299.

Julius Hannink, Thomas Kautz, Cristian F. Pasluosta, Karl-Günter Gaßmann, Jochen Klucken, and Bjoern M. Eskofier. Sensor-Based Gait Parameter Extraction With Deep Convolutional Neural Networks. *IEEE Journal of Biomedical and Health Informatics*, 21(1):85–93, January 2017. ISSN 2168-2208. doi: 10.1109/JBHI.2016.2636456. URL https://ieeexplore.ieee.org/document/7778173. Conference Name: IEEE Journal of Biomedical and Health Informatics.

Harish Haresamudram, Irfan Essa, and Thomas Plötz. Contrastive Predictive Coding for Human Activity Recognition. *Proceedings of the ACM on Interactive, Mobile, Wearable and Ubiquitous Technologies*, 5(2):1–26, June 2021. ISSN 2474-9567. doi: 10.1145/3463506. URL https://dl.acm.org/doi/10.1145/3463506.

D Hazry, M Sofian, and A Zul Azfar. Study of Inertial Measurement Unit Sensor. 2009.

Norman C. Heglund and C. Richard Taylor. Speed, Stride Frequency and Energy Cost Per Stride: How Do They Change With Body Size and Gait? *Journal of Experimental Biology*, 138(1): 301–318, September 1988. ISSN 0022-0949. doi: 10.1242/jeb.138.1.301. URL https://doi.org/10.1242/jeb.138.1.301.

Daniel P. Heil. Predicting Activity Energy Expenditure Using the Actical® Activity Monitor. *Research Quarterly for Exercise and Sport*, 77(1):64–80, March 2006. ISSN 0270-1367. doi: 10.1080/02701367.2006.10599333. URL https://doi.org/10.1080/02701367.2006.10599333. Publisher: Routledge _eprint: https://doi.org/10.1080/02701367.2006.10599333.

Thorsten Hempel, Ahmed A. Abdelrahman, and Ayoub Al-Hamadi. 6d Rotation Representation For Unconstrained Head Pose Estimation. In *2022 IEEE International Conference on Image Processing (ICIP)*, pages 2496–2500, Bordeaux, France, October 2022. IEEE. ISBN 978-1-66549-620-9. doi: 10.1109/ICIP46576.2022.9897219. URL https://ieeexplore.ieee.org/document/9897219/.

Liam Hennessy and Ian Jeffreys. The Current Use of GPS, Its Potential, and Limitations in Soccer. *Strength and Conditioning Journal*, 40:1, March 2018. doi: 10.1519/SSC.0000000000000386.

Jose Heredia-Jimenez and Eva Orantes-Gonzalez. COMPARISON OF THREE DIFFERENT MEASUREMENT SYSTEMS TO ASSESS THE VERTICAL JUMP HEIGHT. *Revista Brasileira de Medicina do Esporte*, 26(2):143–146, April 2020. ISSN 1806-9940, 1517-8692. doi: 10.1590/1517-869220202602185305. URL http://www.scielo.br/scielo.php?script=sci_arttext&pid=S1517-86922020000200143&tlng=en.

US HHS. Physical Activity Guidelines Advisory Committee Report, 2008 to the Secretary of Health and Human Services: (525442010-001), 2008. URL http://doi.apa.org/get-pe-doi.cfm?doi=10.1037/e525442010-001. Institution: American Psychological Association.

Edward T. Howley. Type of activity: resistance, aerobic and leisure versus occupational physical activity. *Medicine & Science in Sports & Exercise*, 33(6):S364, June 2001. ISSN 0195-9131. URL https://journals.lww.com/acsm-msse/fulltext/2001/06001/type_of_activity__resistance,_aerobic_and_leisure.5.aspx.

Shuhei Ishida, Naruhiro Shiozawa, Yoshihisa Fujiwara, and Masaaki Makikawa. Electrocardiogram Measurement during Sleep with Wearing Clothes Using Capacitively-Coupled Electrodes.

In *2007 29th Annual International Conference of the IEEE Engineering in Medicine and Biology Society*, pages 2647–2650, August 2007. doi: 10.1109/IEMBS.2007.4352873. URL https://ieeexplore.ieee.org/document/4352873. ISSN: 1558-4615.

Jihyeok Jang, Ankit Ankit, Jinhyeok Kim, Young Jae Jang, Hye Kim, Jin Kim, and Shuping Xiong. A Unified Deep-Learning Model for Classifying the Cross-Country Skiing Techniques Using Wearable Gyroscope Sensors. *Sensors*, 18:3819, November 2018. doi: 10.3390/s18113819.

Delaram Jarchi, Charence Wong, Richard Kwasnicki, Ben Heller, Garry Tew, and Guang Yang. Gait Parameter Estimation From a Miniaturized Ear-Worn Sensor Using Singular Spectrum Analysis and Longest Common Subsequence. *Biomedical Engineering, IEEE Transactions on*, 61:1261–1273, April 2014. doi: 10.1109/TBME.2014.2299772.

Delaram Jarchi, James Pope, Tracey K. M. Lee, Larisa Tamjidi, Amirhosein Mirzaei, and Saeid Sanei. A Review on Accelerometry-Based Gait Analysis and Emerging Clinical Applications. *IEEE Reviews in Biomedical Engineering*, 11:177–194, 2018. ISSN 1941-1189. doi: 10.1109/RBME.2018.2807182. URL https://ieeexplore.ieee.org/document/8293814. Conference Name: IEEE Reviews in Biomedical Engineering.

Anna Jensen. Introduction to GNSS. In *NKG Summer School*, 2016.

Ning Ji, Hui Zhou, Kaifeng Guo, Oluwarotimi Williams Samuel, Zhen Huang, Lisheng Xu, and Guanglin Li. Appropriate Mother Wavelets for Continuous Gait Event Detection Based on Time-Frequency Analysis for Hemiplegic and Healthy Individuals. *Sensors*, 19(16):3462, January 2019. ISSN 1424-8220. doi: 10.3390/s19163462. URL https://www.mdpi.com/1424-8220/19/16/3462. Number: 16 Publisher: Multidisciplinary Digital Publishing Institute.

Yao-Chiang Kan and Chun-Kai Chen. A Wearable Inertial Sensor Node for Body Motion Analysis. *IEEE Sensors Journal*, 12(3):651–657, March 2012. ISSN 1530-437X, 1558-1748, 2379-9153. doi: 10.1109/JSEN.2011.2148708. URL http://ieeexplore.ieee.org/document/5759066/.

Jordan A. Kerns, Andrew S. Zwart, Pietro S. Perez, Reed D. Gurchiek, and Jeffrey M. McBride. Effect of IMU location on estimation of vertical ground reaction force during jumping. *Frontiers in Bioengineering and Biotechnology*, 11, 2023. ISSN 2296-4185. URL https://www.frontiersin.org/articles/10.3389/fbioe.2023.1112866.

Eugene Kharitonov, Morgane Riviere, Gabriel Synnaeve, Lior Wolf, Pierre-Emmanuel Mazare, Matthijs Douze, and Emmanuel Dupoux. Data Augmenting Contrastive Learning of Speech Representations in the Time Domain. In *2021 IEEE Spoken Language Technology Workshop (SLT)*, pages 215–222, Shenzhen, China, January 2021. IEEE. ISBN 978-1-72817-066-4. doi: 10.1109/SLT48900.2021.9383605. URL https://ieeexplore.ieee.org/document/9383605/.

Igor Khokhlov, Leon Reznik, Justin Cappos, and Rohit Bhaskar. Design of activity recognition systems with wearable sensors. In *2018 IEEE Sensors Applications Symposium (SAS)*, pages 1–6, Seoul, Korea (South), March 2018. IEEE. ISBN 978-1-5386-2092-2. doi: 10.1109/SAS.2018.8336752. URL http://ieeexplore.ieee.org/document/8336752/.

Jussi Kiljander, Roope Sarala, Jari Rehu, Daniel Pakkala, Pekka Pääkkönen, Janne Takalo-Mattila, and Klaus Känsälä. Intelligent Consumer Flexibility Management With Neural Network-Based

Planning and Control. *IEEE Access*, 9:40755–40767, 2021. ISSN 2169-3536. doi: 10.1109/ACCESS.2021.3060871. URL https://ieeexplore.ieee.org/document/9359735. Conference Name: IEEE Access.

Sotiris Kotsiantis. Supervised Machine Learning: A Review of Classification Techniques. *Informatica (Slovenia)*, 31:249–268, January 2007.

Chang June Lee and Jung Keun Lee. IMU-Based Energy Expenditure Estimation for Various Walking Conditions Using a Hybrid CNN–LSTM Model. *Sensors*, 24(2):414, January 2024. ISSN 1424-8220. doi: 10.3390/s24020414. URL https://www.mdpi.com/1424-8220/24/2/414. Number: 2 Publisher: Multidisciplinary Digital Publishing Institute.

Mihyun Lee, Jeong-Hui Park, Myong-Won Seo, Seoung-Ki Kang, and Jung-Min Lee. A New Equation to Estimate Energy Expenditure Using Heart Rate in Children. *Sustainability*, 13 (9):5092, January 2021. ISSN 2071-1050. doi: 10.3390/su13095092. URL https://www.mdpi.com/2071-1050/13/9/5092. Number: 9 Publisher: Multidisciplinary Digital Publishing Institute.

Yin-Shin Lee, Chin-Shan Ho, Yo Shih, Su-Yu Chang, Füle János Róbert, and Tzyy-Yuang Shiang. Assessment of walking, running, and jumping movement features by using the inertial measurement unit. *Gait & Posture*, 41(4):877–881, May 2015. ISSN 0966-6362. doi: 10.1016/j.gaitpost.2015.03.007. URL https://www.sciencedirect.com/science/article/pii/S0966636215000764.

Hyerim Lim, Bumjoon Kim, and Sukyung Park. Prediction of Lower Limb Kinetics and Kinematics during Walking by a Single IMU on the Lower Back Using Machine Learning. *Sensors*, 20(1):130, January 2020. ISSN 1424-8220. doi: 10.3390/s20010130. URL https://www.mdpi.com/1424-8220/20/1/130. Number: 1 Publisher: Multidisciplinary Digital Publishing Institute.

Natalia Lo, Cheng Chih Chen, Dem Lee, Leo Yao, and Jeffrey Lee. Combining Textiles and Electronics: Market Trend and Laundering Testing Challenges of E-Textiles (IMPACT 2018). In *2018 13th International Microsystems, Packaging, Assembly and Circuits Technology Conference (IMPACT)*, pages 169–172, Taipei, Taiwan, October 2018. IEEE. ISBN 978-1-5386-5615-0. doi: 10.1109/IMPACT.2018.8625741. URL https://ieeexplore.ieee.org/document/8625741/.

I. O. Loshkarova. Resting energy expenditure in skilled athletes. *Cherkasy University Bulletin: Biological Sciences Series*, (2):76–83, 2020. ISSN 2518-1211. URL https://bioejournal.cdu.edu.ua/article/view/4074. Number: 2.

Chuanhua Lu, Hideaki Uchiyama, Diego Thomas, Atsushi Shimada, and Rin-ichiro Taniguchi. Indoor Positioning System Based on Chest-Mounted IMU. *Sensors (Basel, Switzerland)*, 19(2): 420, January 2019. ISSN 1424-8220. doi: 10.3390/s19020420. URL https://www.ncbi.nlm.nih.gov/pmc/articles/PMC6359165/.

Kate Lyden, Sarah L. Kozey, John W. Staudenmeyer, and Patty S. Freedson. A comprehensive evaluation of commonly used accelerometer energy expenditure and MET prediction equations. *European Journal of Applied Physiology*, 111(2):187–201, February 2011. ISSN 1439-6327. doi: 10.1007/s00421-010-1639-8. URL https://doi.org/10.1007/s00421-010-1639-8.

Stefan Marković, Milivoj Dopsaj, Sašo Tomažič, Anton Kos, Aleksandar Nedeljković, and Anton Umek. Can IMU Provide an Accurate Vertical Jump Height Estimate? *Applied Sciences*, 11 (24):12025, January 2021. ISSN 2076-3417. doi: 10.3390/app112412025. URL https://www.mdpi.com/2076-3417/11/24/12025. Number: 24 Publisher: Multidisciplinary Digital Publishing Institute.

Guido Mascia and Valentina Camomilla. AN AUTOMATED METHOD FOR THE ESTIMATE OF VERTICAL JUMP POWER THROUGH INERTIAL MEASUREMENT UNITS. 2021.

Rachel Mason, Liam T. Pearson, Gillian Barry, Fraser Young, Oisin Lennon, Alan Godfrey, and Samuel Stuart. Wearables for Running Gait Analysis: A Systematic Review. *Sports Medicine (Auckland, N.z.)*, 53(1):241–268, 2023. ISSN 0112-1642. doi: 10.1007/s40279-022-01760-6. URL https://www.ncbi.nlm.nih.gov/pmc/articles/PMC9807497/.

Jagan Singh Meena, Su Bin Choi, Seung-Boo Jung, and Jong-Woong Kim. Electronic textiles: New age of wearable technology for healthcare and fitness solutions. *Materials Today Bio*, 19:100565, April 2023. ISSN 25900064. doi: 10.1016/j.mtbio.2023.100565. URL https://linkinghub.elsevier.com/retrieve/pii/S259000642300025X.

Sakorn Mekruksavanich, Anuchit Jitpattanakul, Phichai Youplao, and Preecha Yupapin. Enhanced Hand-Oriented Activity Recognition Based on Smartwatch Sensor Data Using LSTMs. *Symmetry*, 12(9):1570, September 2020. ISSN 2073-8994. doi: 10.3390/sym12091570. URL https://www.mdpi.com/2073-8994/12/9/1570. Number: 9 Publisher: Multidisciplinary Digital Publishing Institute.

Sakorn Mekruksavanich, Ponnipa Jantawong, and Anuchit Jitpattanakul. A Deep Learning-based Model for Human Activity Recognition using Biosensors embedded into a Smart Knee Bandage. *Procedia Computer Science*, 214:621–627, 2022. ISSN 18770509. doi: 10.1016/j.procs.2022.11.220. URL https://linkinghub.elsevier.com/retrieve/pii/S1877050922019305.

Paulo Miranda-Oliveira, Marco Branco, and Orlando Fernandes. Accuracy of Inertial Measurement Units When Applied to the Countermovement Jump of Track and Field Athletes. *Sensors*, 22(19):7186, September 2022. ISSN 1424-8220. doi: 10.3390/s22197186. URL https://www.mdpi.com/1424-8220/22/19/7186.

R. Moe-Nilssen. A new method for evaluating motor control in gait under real-life environmental conditions. Part 1: The instrument. *Clinical Biomechanics*, 13(4):320–327, June 1998. ISSN 0268-0033. doi: 10.1016/S0268-0033(98)00089-8. URL https://www.sciencedirect.com/science/article/pii/S0268003398000898.

Tony Monnet, Arnaud Decatoire, and Patrick Lacouture. Comparison of algorithms to determine jump height and flight time from body mounted accelerometers. *Sports Engineering*, 17:11, April 2014. doi: 10.1007/s12283-014-0155-1.

Raynier Montoro-Bombú, Adam Field, Amândio Cúpido Santos, and Luis Rama. Validity and reliability of the Output sport device for assessing drop jump performance. *Frontiers in Bioengineering and Biotechnology*, 10, 2022. ISSN 2296-4185. URL https://www.frontiersin.org/articles/10.3389/fbioe.2022.1015526.

Yuji Morio, Kazuhiro P. Izawa, Yoshitsugu Omori, Hironobu Katata, Daisuke Ishiyama, Shingo Koyama, and Yoshihisa Yamano. The Relationship between Walking Speed and Step Length

in Older Aged Patients. *Diseases*, 7(1):17, March 2019. ISSN 2079-9721. doi: 10.3390/diseases7010017. URL https://www.mdpi.com/2079-9721/7/1/17. Number: 1 Publisher: Multidisciplinary Digital Publishing Institute.

Cao Nan. Research On The Influence Of Wearable Equipment On Sports Under The Background Of Information Technology. In *2022 International Conference on Computer Engineering and Artificial Intelligence (ICCEAI)*, pages 888–890, Shijiazhuang, China, July 2022. IEEE. ISBN 978-1-66546-803-9. doi: 10.1109/ICCEAI55464.2022.00185. URL https://ieeexplore.ieee.org/document/9853482/.

Aaron van den Oord, Yazhe Li, and Oriol Vinyals. Representation Learning with Contrastive Predictive Coding, January 2019. URL http://arxiv.org/abs/1807.03748. arXiv:1807.03748 [cs, stat].

Robert Pettitt, Cherie Pettitt, Chad Cabrera, and Steven Murray. A Theoretical Method of Using Heart Rate to Estimate Energy Expenditure During Exercise. *International Journal of Sports Science & Coaching - INT J SPORTS SCI COACH*, 2, September 2007. doi: 10.1260/174795407782233146.

Minh H. Pham, Morad Elshehabi, Linda Haertner, Silvia Del Din, Karin Srulijes, Tanja Heger, Matthis Synofzik, Markus A. Hobert, Gert S. Faber, Clint Hansen, Dina Salkovic, Joaquim J. Ferreira, Daniela Berg, Álvaro Sanchez-Ferro, Jaap H. van Dieën, Clemens Becker, Lynn Rochester, Gerhard Schmidt, and Walter Maetzler. Validation of a Step Detection Algorithm during Straight Walking and Turning in Patients with Parkinson's Disease and Older Adults Using an Inertial Measurement Unit at the Lower Back. *Frontiers in Neurology*, 8, September 2017. ISSN 1664-2295. doi: 10.3389/fneur.2017.00457. URL https://www.frontiersin.org/journals/neurology/articles/10.3389/fneur.2017.00457/full. Publisher: Frontiers.

Polar Oy. Polar M460 User Manual | Heart Rate Zones, 2021. URL https://support.polar.com/e_manuals/M460/Polar_M460_user_manual_English/Content/Heart_rate_Zones.htm.

Manju Rana and Vikas Mittal. Wearable Sensors for Real-Time Kinematics Analysis in Sports: A Review. *IEEE Sensors Journal*, 21(2):1187–1207, January 2021. ISSN 1530-437X, 1558-1748, 2379-9153. doi: 10.1109/JSEN.2020.3019016. URL https://ieeexplore.ieee.org/document/9174823/.

Pedro Reche-Soto, Donaldo Cardona-Nieto, Arturo Diaz-Suarez, Alejandro Bastida-Castillo, Carlos Gomez-Carmona, Javier Garcia-Rubio, and Jose Pino-Ortega. Player Load and Metabolic Power Dynamics as Load Quantifiers in Soccer. *Journal of Human Kinetics*, 69:259–269, October 2019. ISSN 1640-5544. doi: 10.2478/hukin-2018-0072. URL https://www.ncbi.nlm.nih.gov/pmc/articles/PMC6815086/.

Mateo Rico-Garcia, Juan Botero-Valencia, and Ruber Hernández-García. Vertical Jump Data from Inertial and Optical Motion Tracking Systems. *Data*, 7(8), 2022. ISSN 2306-5729. doi: 10.3390/data7080116. URL https://www.mdpi.com/2306-5729/7/8/116.

Markel Rico-González, Daniel Puche-Ortuño, Filipe Manuel Clemente, Rodrigo Aquino, and José Pino-Ortega. The Most Demanding Exercise in Different Training Tasks in Professional Female Futsal: A Mid-Season Study through Principal Component Analysis. *Healthcare*, 10(5):838,

May 2022. ISSN 2227-9032. doi: 10.3390/healthcare10050838. URL https://www.mdpi.com/2227-9032/10/5/838.

Sietse Rispens. Identification of Fall Risk Predictors in Daily Life Measurements. URL https://journals.sagepub.com/doi/epub/10.1177/1545968314532031.

Alex Rowlands, Francois Fraysse, Mike Catt, Victoria Stiles, Rebecca Stanley, Roger Eston, and Tim Olds. Comparability of Measured Acceleration from Accelerometry-Based Activity Monitors. *Medicine and science in sports and exercise*, 47, May 2014. doi: 10.1249/MSS.0000000000000394.

Stephen Roy and Jean Mccrory. Validation of Maximal Heart Rate Prediction Equations Based on Sex and Physical Activity Status. *International Journal of Exercise Science*, 8(4):318–330, October 2015. ISSN 1939-795X. URL https://www.ncbi.nlm.nih.gov/pmc/articles/PMC4831892/.

Martin Runge, Jörn Rittweger, Cosimo Roberto Russo, Hans Schiessl, and Dieter Felsenberg. Is muscle power output a key factor in the age-related decline in physical performance? A comparison of muscle cross section, chair-rising test and jumping power. *Clinical Physiology and Functional Imaging*, 24(6):335–340, 2004. ISSN 1475-097X. doi: 10.1111/j.1475-097X.2004.00567.x. URL https://onlinelibrary.wiley.com/doi/abs/10.1111/j.1475-097X.2004.00567.x. _eprint: https://onlinelibrary.wiley.com/doi/pdf/10.1111/j.1475-097X.2004.00567.x.

Graciela Sanchez, Cristian Castro, and David Mauricio. Roadmap of projects for the design of clothing with wearable technology. In *2022 IEEE Engineering International Research Conference (EIRCON)*, pages 1–4, Lima, Peru, October 2022. IEEE. ISBN 978-1-66545-082-9. doi: 10.1109/EIRCON56026.2022.9934091. URL https://ieeexplore.ieee.org/document/9934091/.

Simen Sandmæl and Terje Dalen. Comparison of GPS and IMU systems for total distance, velocity, acceleration and deceleration measurements during small-sided games in soccer. *Cogent Social Sciences*, 9(1):2209365, December 2023. ISSN null. doi: 10.1080/23311886.2023.2209365. URL https://doi.org/10.1080/23311886.2023.2209365. Publisher: Cogent OA _eprint: https://doi.org/10.1080/23311886.2023.2209365.

Soheil Sarabandi and Federico Thomas. Accurate Computation of Quaternions from Rotation Matrices. In Jadran Lenarcic and Vincenzo Parenti-Castelli, editors, *Advances in Robot Kinematics 2018*, volume 8, pages 39–46. Springer International Publishing, Cham, 2019. ISBN 978-3-319-93187-6 978-3-319-93188-3. doi: 10.1007/978-3-319-93188-3_5. URL http://link.springer.com/10.1007/978-3-319-93188-3_5. Series Title: Springer Proceedings in Advanced Robotics.

Edward S Sazonov, George Fulk, James Hill, Yves Schutz, and Raymond Browning. Monitoring of Posture Allocations and Activities by a Shoe-Based Wearable Sensor. *IEEE Transactions on Biomedical Engineering*, 58(4):983–990, April 2011. ISSN 0018-9294, 1558-2531. doi: 10.1109/TBME.2010.2046738. URL http://ieeexplore.ieee.org/document/5447796/.

Kathryn H. Schmitz, Margarita Treuth, Peter Hannan, Robert Mcmurray, Kimberly B. Ring, Diane Catellier, and Russ Pate. Predicting Energy Expenditure from Accelerometry Counts in Adolescent Girls. *Medicine and science in sports and exercise*, 37(1):155–161, January 2005.

ISSN 0195-9131. doi: 10.1249/01.MSS.0000150084.97823.F7. URL https://www.ncbi.nlm.nih.gov/pmc/articles/PMC2491725/.

Philip J. Schneider and David H. Eberly. *Geometric tools for computer graphics*. The Morgan Kaufmann series in computer graphics and geometric modeling. Boston : Morgan Kaufmann Publishers, Amsterdam, 2003. ISBN 978-1-55860-594-7.

Monica P Sikka, Suresh Kumar, and Samridhi Garg. Smart Textiles for Biomedical Applications. In *2023 Joint International Conference on Digital Arts, Media and Technology with ECTI Northern Section Conference on Electrical, Electronics, Computer and Telecommunications Engineering (ECTI DAMT & NCON)*, pages 511–516, Phuket, Thailand, March 2023. IEEE. ISBN 9798350396546. doi: 10.1109/ECTIDAMTNCON57770.2023.10139695. URL https://ieeexplore.ieee.org/document/10139695/.

C. Skazalski, R. Whiteley, C. Hansen, and R. Bahr. A valid and reliable method to measure jump-specific training and competition load in elite volleyball players. *Scandinavian Journal of Medicine & Science in Sports*, 28(5):1578–1585, 2018. ISSN 1600-0838. doi: 10.1111/sms.13052. URL https://onlinelibrary.wiley.com/doi/abs/10.1111/sms.13052. _eprint: https://onlinelibrary.wiley.com/doi/pdf/10.1111/sms.13052.

Alex Smola and S.V.N Vishwanathan. *Principles of constraint programming*. Cambridge Univ. Pr, Cambridge, digitally print. version (with minor corr.) edition, 2009. ISBN 978-0-521-82583-2 978-0-521-12549-9.

Wei Su and Jian Feng. EFFECTS OF DEEP JUMPING ON EXPLOSIVE STRENGTH IN THE LOWER LIMBS OF ATHLETES. *Revista Brasileira de Medicina do Esporte*, 29: e2022_0573, 2023. ISSN 1806-9940, 1517-8692. doi: 10.1590/1517-8692202329012022_0573. URL http://www.scielo.br/scielo.php?script=sci_arttext&pid=S1517-86922023000100980&tlng=en.

Ilya Sutskever, Oriol Vinyals, and Quoc V Le. Sequence to Sequence Learning with Neural Networks. In *Advances in Neural Information Processing Systems*, volume 27. Curran Associates, Inc., 2014. URL https://papers.nips.cc/paper_files/paper/2014/hash/a14ac55a4f27472c5d894ec1c3c743d2-Abstract.html.

Ada Szmygin, Marcin Wojtowicz, Żaneta Świderska Chadaj, and Radosław Roszczyk. Prediction of athletes' performance results using machine learning algorithms. In *2023 24th International Conference on Computational Problems of Electrical Engineering (CPEE)*, pages 1–5, Grybów, Poland, September 2023. IEEE. ISBN 9798350330342. doi: 10.1109/CPEE59623.2023.10285142. URL https://ieeexplore.ieee.org/document/10285142/.

Daniel Tazartes. An historical perspective on inertial navigation systems. In *2014 International Symposium on Inertial Sensors and Systems (ISISS)*, pages 1–5, February 2014. doi: 10.1109/ISISS.2014.6782505. URL https://ieeexplore.ieee.org/document/6782505.

Philippe Terrier and Olivier Dériaz. Kinematic variability, fractal dynamics and local dynamic stability of treadmill walking. *Journal of NeuroEngineering and Rehabilitation*, 8(1):12, February 2011. ISSN 1743-0003. doi: 10.1186/1743-0003-8-12. URL https://doi.org/10.1186/1743-0003-8-12.

A. Thorstensson and H. Roberthson. Adaptations to changing speed in human locomotion: speed of transition between walking and running. *Acta Physiologica Scandinavica*,

131(2):211–214, 1987. ISSN 1365-201X. doi: 10.1111/j.1748-1716.1987.tb08228.x. URL https://onlinelibrary.wiley.com/doi/abs/10.1111/j.1748-1716.1987.tb08228.x. _eprint: https://onlinelibrary.wiley.com/doi/pdf/10.1111/j.1748-1716.1987.tb08228.x.

Tina, Anmol Kumar Sharma, Siddharth Tomar, and Kapil Gupta. Various Approaches of Human Activity Recognition: A Review. In *2021 5th International Conference on Computing Methodologies and Communication (ICCMC)*, pages 1668–1676, Erode, India, April 2021. IEEE. ISBN 978-1-66540-360-3. doi: 10.1109/ICCMC51019.2021.9418226. URL https://ieeexplore.ieee.org/document/9418226/.

Emil Toft Nielsen, Peter Bo Jørgensen, Inger Mechlenburg, and Henrik Sørensen. Validation of an inertial measurement unit to determine countermovement jump height. *Asia-Pacific Journal of Sports Medicine, Arthroscopy, Rehabilitation and Technology*, 16:8–13, April 2019. ISSN 2214-6873. doi: 10.1016/j.asmart.2018.09.002. URL https://www.sciencedirect.com/science/article/pii/S2214687318300189.

Justin Trautmann, Lin Zhou, Clemens Markus Brahms, Can Tunca, Cem Ersoy, Urs Granacher, and Bert Arnrich. TRIPOD—A Treadmill Walking Dataset with IMU, Pressure-Distribution and Photoelectric Data for Gait Analysis. *Data*, 6(9):95, September 2021. ISSN 2306-5729. doi: 10.3390/data6090095. URL https://www.mdpi.com/2306-5729/6/9/95. Number: 9 Publisher: Multidisciplinary Digital Publishing Institute.

R Usubamatov, Abdykerimova D, and Dotalieva Z. A Mathematical Model for an Acceleration of a Rotating Object about a Fixed Axis. *Journal of Applied & Computational Mathematics*, 7(2):1–4, 2018. ISSN 2168-9679. doi: 10.4172/2168-9679.1000394. URL https://www.hilarispublisher.com/abstract/a-mathematical-model-for-an-acceleration-of-a-rotating-object-about-a-fixed-axis-28782.html. Publisher: Hilaris SRL.

Emil Valchinov, Athanasios Antoniou, Konstantinos Rotas, and Nicolas Pallikarakis. Wearable ECG system for health and sports monitoring. In *2014 4th International Conference on Wireless Mobile Communication and Healthcare - Transforming Healthcare Through Innovations in Mobile and Wireless Technologies (MOBIHEALTH)*, pages 63–66, November 2014. doi: 10.1109/MOBIHEALTH.2014.7015910. URL https://ieeexplore.ieee.org/document/7015910.

Matthew C. Varley, Ian H. Fairweather, and 2 Aughey1, Robert J. Validity and reliability of GPS for measuring instantaneous velocity during acceleration, deceleration, and constant motion. *Journal of Sports Sciences*, 30(2):121–127, January 2012. ISSN 0264-0414. doi: 10.1080/02640414.2011.627941. URL https://doi.org/10.1080/02640414.2011.627941. Publisher: Routledge _eprint: https://doi.org/10.1080/02640414.2011.627941.

Eduardo Velloso, Andreas Bulling, Hans Gellersen, Wallace Ugulino, and Hugo Fuks. Qualitative activity recognition of weight lifting exercises. In *Proceedings of the 4th Augmented Human International Conference*, AH '13, pages 116–123, New York, NY, USA, March 2013. Association for Computing Machinery. ISBN 978-1-4503-1904-1. doi: 10.1145/2459236.2459256. URL https://dl.acm.org/doi/10.1145/2459236.2459256.

Pema Wangmo, Mannat Uppal, Oinam Robita Chanu, Amritaa Easwaran, and Goli Ramyavani. Dual Electrodes System for acquisition of ECG Waveform. In *2020 International Conference on*

Communication and Signal Processing (ICCSP), pages 0607–0612, Chennai, India, July 2020. IEEE. ISBN 978-1-72814-988-2. doi: 10.1109/ICCSP48568.2020.9182278. URL https://ieeexplore.ieee.org/document/9182278/.

Wei Xia, Yu Zhou, Yinfeng Fang, and Honghai Liu. ECG-Enhanced Multi-sensor Solution for Wearable Sports Devices. In *2018 IEEE International Conference on Systems, Man, and Cybernetics (SMC)*, pages 1939–1944, Miyazaki, Japan, October 2018. IEEE. ISBN 978-1-5386-6650-0. doi: 10.1109/SMC.2018.00335. URL https://ieeexplore.ieee.org/document/8616331/.

Fraser Young, Rachel Mason, Conor Wall, Rosie Morris, Samuel Stuart, and Alan Godfrey. Examination of a foot mounted IMU-based methodology for a running gait assessment. *Frontiers in Sports and Active Living*, 4, 2022. ISSN 2624-9367. URL https://www.frontiersin.org/articles/10.3389/fspor.2022.956889.

Shi Zhang, She Lihuang, and Guohua Wang. Wayback Machine, August 2017. URL https://web.archive.org/web/20170809152315/http://nlpr-web.ia.ac.cn/2009papers/kz/gh14.pdf.

Jichen Zhu. The Acquisition and Application of ECG in Wearable Devices. In *2022 International Conference on Electronics and Devices, Computational Science (ICEDCS)*, pages 175–178, September 2022. doi: 10.1109/ICEDCS57360.2022.00045. URL https://ieeexplore.ieee.org/document/9997041.

Zetao Zhu, Huining Li, Jian Xiao, Wenyao Xu, and Ming-Chun Huang. A fitness training optimization system based on heart rate prediction under different activities. *Methods*, 205:89–96, September 2022. ISSN 1046-2023. doi: 10.1016/j.ymeth.2022.06.006. URL https://www.sciencedirect.com/science/article/pii/S1046202322001463.

Wiebren Zijlstra and At Hof. Displacement of the pelvis during human walking: Experimental data and model predictions. *Gait & Posture - GAIT POSTURE*, 6:249–262, December 1997. doi: 10.1016/S0966-6362(97)00021-0.

Wiebren Zijlstra and At L Hof. Assessment of spatio-temporal gait parameters from trunk accelerations during human walking. *Gait & Posture*, 18(2):1–10, October 2003. ISSN 0966-6362. doi: 10.1016/S0966-6362(02)00190-X. URL https://www.sciencedirect.com/science/article/pii/S096663620200190X.

Markus Zrenner, Stefan Gradl, Ulf Jensen, Martin Ullrich, and Bjoern M. Eskofier. Comparison of Different Algorithms for Calculating Velocity and Stride Length in Running Using Inertial Measurement Units. *Sensors*, 18(12):4194, December 2018. ISSN 1424-8220. doi: 10.3390/s18124194. URL https://www.mdpi.com/1424-8220/18/12/4194. Number: 12 Publisher: Multidisciplinary Digital Publishing Institute.

Appendix A

IMU Specifications

Device	Resolution	Frequency Sampling	Scale
ECG	16 bit	1000 Hz	+/- 1.25mV
IMU-Accelerometer	16 bit	1000 Hz	+/-8g
IMU-Gyroscope	16 bit	1000 Hz	+/- 500dps

Table A.1: IMU Plux Specifications

Device	Range	Noise Density
Accelerometer	+10 g	60 ug/sqrt(Hz)
Gyroscope	2000 (dps)	0.007°/s/sqrt(Hz)
Magnetometer	+/-8T	1 mT

Table A.2: IMU Plux Biosignals Operating Ranges

Device	Range	Noise /Sensitivity
IMU-Gyroscope	±250 (dps) ±500 (dps) ±1000 (dps) ±2000 (dps)	0.01 (Noise)
IMU-Accelerometer	±2g ±4g ±8g ±16g	4000 (Sensitivity LSB/g)

Table A.3: IMU MPU-9250 Operating Ranges

Device	**Range**	**Frequency**
Accelerometer	±16g	512 Hz
Gyroscope	±2000°/s	512 Hz
Magnetometer	+50mT	256 Hz

Table A.4: IMU Physilog®5 Operating Ranges